Published Online: 13 January, 2014 | Supp Info: http://doi.org/10.1085/jgp.201311007

Research Article

Calcium-dependent stoichiometries of the $KCa_{2.2}$ (SK) intracellular domain/calmodulin complex in solution

D. Brent Halling,[1,2] Sophia A. Kenrick,[3] Austen F. Riggs,[1] and Richard W. Aldrich[1,2]

[1]Department of Neuroscience, [2]Center for Learning and Memory, The University of Texas at Austin, Austin, TX 78712
[3]Wyatt Technology Corporation, Santa Barbara, CA 93117

Ca^{2+} activates SK Ca^{2+}-activated K^+ channels through the protein Ca^{2+} sensor, calmodulin (CaM). To understand how SK channels operate, it is necessary to determine how Ca^{2+} regulates CaM binding to its target on SK. Tagless, recombinant SK peptide (SKp), was purified for binding studies with CaM at low and high Ca^{2+} concentrations. Composition gradient multi-angle light scattering accurately measures the molar mass, stoichiometry, and affinity of protein complexes. In 2 mM Ca^{2+}, SKp and CaM bind with three different stoichiometries that depend on the molar ratio of SKp:CaM in solution. These complexes include 28 kD 1SKp/1CaM, 39 kD 2SKp/1CaM, and 44 kD 1SKp/2CaM. A 2SKp/2CaM complex, observed in prior crystallographic studies, is absent. At <5 nM Ca^{2+}, 1SKp/1CaM and 2SKp/1CaM were observed; however, 1SKp/2CaM was absent. Analytical ultracentrifugation was used to characterize the physical properties of the three SKp/CaM stoichiometries. In high Ca^{2+}, the sedimentation coefficient is smaller for a 1SKp:1CaM solution than it is for either 2SKp:1CaM or 1SKp:2CaM. At low Ca^{2+} and at >100 µM protein concentrations, a molar excess of SKp over CaM causes aggregation. Aggregation is not observed in Ca^{2+} or with CaM in molar excess. In low Ca^{2+} both 1SKp:1CaM and 1SKp:2CaM solutions have similar sedimentation coefficients, which is consistent with the absence of a 1SKp/2CaM complex in low Ca^{2+}. These results suggest that complexes with stoichiometries other than 2SKp/2CaM are important in gating.

The Journal of General Physiology

INTRODUCTION

Ca^{2+} signals initiate diverse responses in a cell, and Ca^{2+} can regulate its own intracellular concentration. Ca^{2+} influx through voltage-dependent Ca^{2+} channels (VDCCs) can be modulated by cell-membrane repolarization through activation of Ca^{2+}-activated K^+ channels such as the small-conductance Ca^{2+}-activated (SK2) K^+ channel (Banks et al., 1979). A major physiological role of SK2 channels is to restore an excited cell back to its resting state in response to increases in local intracellular Ca^{2+} concentration.

The SK2 protein binds Ca^{2+} through a ubiquitous cell regulator, calmodulin (CaM; Xia et al., 1998). CaM, which can bind Ca^{2+} at four sites, participates in essential Ca^{2+} sensing roles for many diverse proteins (Jurado et al., 1999). The energetics of SK activity are controlled by the dynamic coupling between Ca^{2+} binding to CaM, CaM binding to SK, and the open probability of SK. It has been shown by x-ray crystallography that CaM can bind to a recombinant SK2 fragment with a somewhat extended conformation, having a C-shaped configuration (Schumacher et al., 2001; Fig. 1 A). Several structures have been obtained with CaM bound to various targets (Yamniuk and Vogel, 2004; Halling et al., 2006), yet the conformation of CaM bound to SK is unique. In the crystal, antiparallel CaMs and antiparallel SK peptides form a dimeric complex, with a stoichiometry of 2 SK peptide (SKp) to 2 CaM, which we will denote as 2SKp/2CaM. Ca^{2+} ions are only bound to the N-lobe binding sites, and the C-lobe sites are unoccupied even at high Ca^{2+} concentrations. Recently, the 2SKp/2CaM stoichiometry was supported by new crystal structures of the SKp–CaM complex. One structure contains an alternatively spliced SK variant (Zhang et al., 2012a), and other structures were solved with either phenyl urea or 1-ethylbenzimidazolinone (1-EBIO) as CaM binding agonists at the protein–protein interface (Zhang et al., 2012b). It has been argued that this 2SKp/2CaM configuration represents the conformation that the SK C termini assume in the full-length SK channel when activated (Schumacher et al., 2001).

The structure inspired a mechanistic hypothesis for channel gating involving two CaM molecules that bridge two SK fragments upon Ca^{2+} binding to the N-lobe to lock the channel in a conformation that favors opening. We will refer to this as the 2/2 gating model. If all subunits are functioning during gating, SKs are proposed to assemble as dimers of dimerized subunits with twofold symmetry (Fig. 1 B). This contrasts with other homotetrameric

Correspondence to Richard W. Aldrich: raldrich@austin.utexas.edu

Abbreviations used in this paper: CaM, calmodulin; CG-MALS, composition gradient MALS; MALS, multiangle light scattering; SEC, size-exclusion column; SKp, SK peptide; SV-AUC, sedimentation velocity in an analytical centrifuge; VDCC, voltage-dependent Ca^{2+} channel; vHW, van Holde-Weischet analysis.

K^+ channels that generally assemble with fourfold symmetry (MacKinnon, 2003). Because CaM binds in both the absence and presence of Ca^{2+}, CaM has been considered to be constitutively associated with SK (Xia et al., 1998; Keen et al., 1999; Schumacher et al., 2001; Wissmann et al., 2002). However, no studies have shown that either the SK affinity for CaM or the structure of the complex are invariant with Ca^{2+} concentration. The open probability of the channel will depend on Ca^{2+} occupation of CaM, the affinity of CaM for SK at various Ca^{2+} occupancies, and the Ca^{2+}-dependent conformations of CaM, SK, and their complex. At present, the crystal structures provide only one possible conformation in the presence of Ca^{2+}. There is therefore a need to test the 2/2 gating model in the presence and absence of Ca^{2+}

We used multiple independent approaches to measure the stoichiometries and the molar masses and affinities of the complexes that form between SKp and CaM in high and low Ca^{2+}. Multiangle light scattering (MALS) quantifies the scattered light intensity of a molecule at many angles to measure the molar mass (Debye, 1944; Zimm, 1948; Wyatt, 1993). Composition gradient MALS (CG-MALS) includes a recent advance in the technique to precisely mix different protein compositions and to measure the apparent molar mass at various molar ratios. Performing analyses as a function of composition increases the capability of MALS so that stoichiometry and protein affinities can be accurately measured (Attri and Minton, 2005). Sedimentation velocity measurements using analytical centrifugation have the potential to measure both sedimentation and diffusion rate constants to provide information on the shape or hydration state in addition to estimating the mass of the molecule (Van Holde and Weischet, 1978; Laue and Stafford, 1999; Schuck, 2000; Brookes et al., 2010; Demeler et al., 2010). These methods provide interpretable conclusions about the stoichiometries and the affinities of SKp and CaM, an important step in characterizing and measuring the energetics of SK gating.

MATERIALS AND METHODS

Reagents

The protein expression clones for the mammalian CaM constructs were provided by S. Hamilton (Baylor College of Medicine, Houston, TX). J. Adelman (Vollum Institute, Portland, OR) provided the clone for the *Rattus norvegicus* SKp of SK2, which contains a C-terminal histidine tag (His-SKp). The human protein sequence of SK2 is identical in this region. Reagents used for buffers were minimal American Chemical Society quality and purchased from Sigma-Aldrich unless otherwise indicated.

Protein expression and purification

The SKp sequence is identical to the sequence used in previous studies, minus the histidine tag (Schumacher et al., 2001). The sequence includes residues R396 to Q487, with extra methionine and glycine residues inserted at the amino terminus. PCR mutagenesis was used to insert a stop codon in the cDNA immediately before the histidine tag to create a construct that could express the SK2 peptide without a tag (SKp). For protein expression, BL21 (DE3) *Escherichia coli* cells (Merck) were chemically transformed with CaM cDNA alone or with a 2:1 CaM/SKp molar ratio of cDNA together. The CaM construct confers carbenicillin resistance

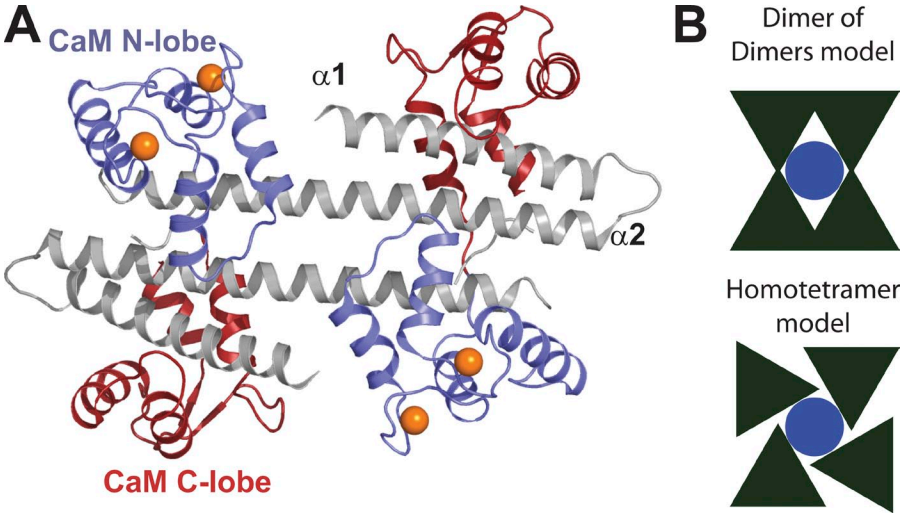

Figure 1. SK gating by CaM. (A) Cartoon ribbons representing a complex of two "antiparallel" CaM molecules (blue, N-lobe; red, C-lobe) and two "antiparallel" SKp-histidine tagged protein (gray; Schumacher et al., 2001; Protein Data Bank accession no. 1G4Y). Ca^{2+} is shown as orange spheres. Only the N-lobe of CaM has Ca^{2+} bound, and it engages α-2 of a SKp-histidine. The Ca^{2+}-free C-lobe wraps around two SK fragment helices near to where α-1 bends into α-2. (B) Arrangement of subunits of SK channel based on interpretation from crystal structure. Dark green triangles represent SK subunits. The blue circle represents the central pore. The top panel represents a schematic view looking toward the membrane at a channel that is formed from a dimer of dimerized subunits; each dimer is formed when CaM molecules form intersubunit contacts. Note this model has only twofold symmetry around the pore. The bottom panel depicts a typical arrangement of four channel subunits with a fourfold symmetry about the central pore.

as a selection marker, whereas SKp confers kanamycin resistance. To select for BL21 (DE3) cells with both CaM and SKp, colonies were selected from plates that contained both antibiotics. A single colony was selected for a shaking overnight starter culture in Luria broth containing both 100 µg/ml carbenicillin and 50 µg/ml kanamycin. The next day, the starter culture was diluted to 1.5 liters and was grown to an optical density of 0.6–0.8 at 37°C, maintaining 250 rpm, then induced with 0.5 mM isopropyl β-D-1-thiogalactopyranoside and incubated in the shaker for 3 h before harvesting by centrifugation. The pellets were fully suspended at room temperature in 25 ml B-Per (Thermo Fisher Scientific) containing 100 U/ml Benzonase (Merck), 15 mM dithiothreitol (Roche), 0.5 mg/ml lysozyme (MP Biomedicals), Complete Mini, EDTA-free protease inhibitor tablets (Roche), and 2 mM $MgCl_2$. All subsequent steps were performed at 4°C. The suspension was centrifuged at 30,000 *g* for 30 min. The pellet was saved on ice. The pellet with SKp was homogenized and solubilized in 6 M Guanidine-HCl followed by centrifugation for 30 min at 50,000 *g*. The supernatant contains SKp, and it was dialyzed against 4 liters of 20 mM HEPES and 150 mM NaCl, pH 7.0, for 4 h. The sample was centrifuged again at 50,000 *g* for 30 min. The supernatant was loaded onto a 20 ml HiPrep CM FF 16/10 (GE Healthcare) cation exchange column. Elution was performed by a gradient to 2 M NaCl and 20 mM HEPES, pH 7.0. CaM was purified according to established procedures that use ammonium sulfate precipitation and phenyl Sepharose chromatography (Marshak, 1996). As a final step in both the CaM and SKp procedures, the samples were concentrated and 5 ml of the protein solutions were separately passed through a HiLoad 16/60 Superdex 75 pg column (GE Healthcare). Purified proteins were stored at −80°C and thawed the same day of experiments. Before experiments, SKp and CaM were filtered through 0.45-µm pores in a centrifuge at 10,000 *g* for 10 min to remove particulates.

SKp and CaM mass spectrometry

SKp was dialyzed against 1 mM HEPES, pH 7.0, and CaM was dialyzed against 1 mM Tris, pH 7.4, and 1 mM EDTA. A total of 1.5 nmol of each protein sample was sent to The University of Texas protein core facility for analysis. High protein purity for both SKp and CaM samples was confirmed by liquid chromatography–electrospray ionization/multiple-stage mass spectrometry (LC-ESI/MS/MS) in a hybrid triple quadrupole-linear ion trap (QTrap; ABI Sciex 4000) with Shimadzu Prominence analytical HPLC at the Protein and Metabolite Analysis Facility at The University of Texas at Austin. SKp appears as a single peptide having a mass of 11,015 D in LC-ESI/MS/MS. These data agree with the predicted mass of SKp, assuming nominal N-terminal methionine processing, of 11,014 D. The spectra suggest that up to three sodium atoms may bind, creating minor peaks at 11,037 and 11,060 D. Additionally, small but significant peaks are observed at 11,194 D and 11,274 D, which suggests a small amount of protein modification. The differences in mass are 179 and 258 D. These masses are consistent with gluconoylation at the N terminus of the peptide (Geoghegan et al., 1999; Aon et al., 2008). These studies suggest that gluconoylation occurs during the overexpression of recombinant peptides in bacteria, especially for histidine-tagged proteins. The SKp peptide has no histidine tag, as verified by mass spectrometry. If the modification is at the N terminus, it would be far enough from the putative CaM-binding residues of SKp that it would most likely be solvent exposed (Zhang et al., 2013). SKp has a theoretical isoelectric point of 10.6, perhaps suggesting that positive charges augment gluconoylation. The amount of gluconoylation appears to vary a little among different protein preparations, so greater numbers of experiments were performed across different batches of purification. Although not directly tested, we assume that any effect gluconoylation has on our studies is small.

CaM in 1 mM EDTA and 1 mM Tris, pH 7.4, was also evaluated by similar LC-ESI/MS/MS analyses. There is a dominant peak at 16,708 D, which is virtually the same as the predicted mass of 16,706 D for monomeric CaM. Multiple minor peaks corresponding to adducts of Na^+, K^+, and/or Ca^{2+} were observed.

Determination of protein concentration

The Edelhoch method for measuring protein concentration was followed (Edelhoch, 1967). Dry protein was weighed on a balance that is accurate to ∼0.01 mg. CaM peptides with the sequences GYISAAE and VNYEE were synthesized and purified on Sep-Pak (Waters). Full-length CaM was dialyzed for 2 d with six exchanges against 4 liters water/exchange. Samples were frozen and then lyophilized under 2×10^{-3} mbar vacuum at −115°C and then heated to 100°C for 24 h to enhance the removal of water. Immediately upon completion of drying, samples were cap sealed to prevent moisture from being absorbed by samples. Masses were measured on an XP105DR balance (Mettler Toledo). Experimental variability for mass measurements was determined to be 0.04 mg. 8 M urea (Macron Chemicals) was used to dissolve all samples, as pure water was less effective. Dissolved samples were weighed. The solution was then ready for UV spectroscopy to determine the extinction coefficient of a known quantity of protein. Spectra from 240–350 nm were collected on a spectrophotometer (DU640; Beckman Coulter). The extinction coefficient (ε) was determined using the relation: $\varepsilon = A/c$, where A is the maximal absorbance near 280 nm with a path length of 10 mm and c is the protein concentration. The measured extinction coefficient for CaM we used for our studies is 3,020 ± 120 $M^{-1}cm^{-1}$ at 276 nm. Propagation of error was used for determining experimental variability. SKp has a tryptophan and its extinction coefficient was measured to be 7,200 ± 300 $M^{-1}cm^{-1}$.

CG-MALS

CG-MALS was performed using Calypso II (Wyatt Technology), a triple syringe pump system, to deliver sample and solvent to a HELEOS II MALS detector (Wyatt Technology) and an inline UV/Vis dual wavelength detector (2487; Waters). Samples were dialyzed into 9 mM HEPES, 100 mM NaCl, and 2 mM $CaCl_2$, pH 7.0, or into 5 mM HEPES, 100 mM NaCl, and 5 mM EGTA. The free Ca^{2+} in a solution of 5 mM EGTA was estimated to be <5 nM. We define 2 mM Ca^{2+} as saturating Ca^{2+} and <5 nM to be zero Ca^{2+}. The free Ca^{2+} in solutions containing EGTA was estimated using MaxChelator version 1.3 (Schoenmakers et al., 1992). Buffers were filtered through 0.1 µm porous membrane. Proteins were diluted to predetermined stock concentrations and filtered to 0.02 µm with a syringe-tip filter (Whatman Anotop; GE Healthcare) before loading into Calypso II, which has 0.03-µm polyethersulfone inline filters (Sterlitech). After each injection, the flow was stopped for 60–180 s to allow for any association or dissociation kinetics. Two gradient protocols were used for proteins in Ca^{2+} buffer, whereas just one protocol was followed for proteins in EGTA buffer. The "self+hetero-association" method consists of two single-component concentration gradients to assess self-association and a dual-component "crossover" composition gradient to assess the hetero-association behavior (Fig. 2 A). For each composition, 0.7 ml of protein solution at the appropriate composition was injected into the UV and MALS detectors. The flow was stopped for 60–180 s to allow the solution to come to equilibrium in the flow cell. During the hetero-association gradient, the concentration of CaM was increased while the concentration of SKp was simultaneously decreased to sample 13–15 different SKp/CaM ratios. The "dual crossover" protocol consisted of two mirror-image hetero-association gradients, each with 15 different concentrations of CaM and SKp, to replicate the binding conditions in the "self+hetero" method and to rule out hardware error (Fig. 2 B).

The analysis of CG-MALS data has been previously described (Attri and Minton, 2005). For a system of two interacting species A and B in a dilute solution, the light scattering intensity as a function of composition can be written as

$$\frac{R}{K^*} = M_A{}^2\left[A_{inc}\right] + M_B{}^2\left[B_{inc}\right] + \sum_{i,j}\left(iM_A + jM_B\right)^2\left[A_iB_j\right],$$

where R is the excess Rayleigh ratio, and M_A and M_B are the molar mass of each monomer. K* is an optical constant where

$$K^* = \frac{4\pi^2(dn/dc)^2 n_o}{N_A\lambda_o{}^4},$$

consisting of the laser wavelength λ, refractive index of the solution n_o, Avogadro's number N_A, and the differential refractive index of the molecule, dn/dc (Wyatt, 1993). The dn/dc is how much the refractive index of a solution varies for a given increment of concentration and is assumed to be 0.185 ml/g (Barer and Joseph, 1954). The indices i and j represent the stoichiometric numbers of A and B in the A_iB_j complex, with A_1B_0 and A_0B_1 representing the competent monomers of A and B, respectively, and $[A_iB_j]$ represents the molar concentration of the A_iB_j complex. The terms A_{inc} and B_{inc} refer to "incompetent" protein concentrations that are incapable of binding due to artifacts of protein purification, modification, or misfolding (Attri and Minton, 2005).

The concentration of each A_iB_j species is related to the total competent molar concentration of A and B ($[A]_{total}$ and $[B]_{total}$) by the equilibrium association constant, K_{ij}, and the conservation of mass as follows:

$$K_{i,j} = \frac{\left[A_iB_j\right]}{[A]^i[B]^j}$$

$$[A]_{total} = \sum_i i\left[A_iB_j\right], \quad [B]_{total} = \sum_j j\left[A_iB_j\right].$$

If we let f_A equal the fraction of A that is competent and f_B equal the fraction of B that is competent, then we also have the following relations in the absence of ligand:

$$[A]_{total} = f_A[A]_{Measured}.$$

It follows that

$$[A]_{inc} = (1 - f_A)[A]_{Measured}.$$

The concentrations for [B] and $[B]_{Inc.}$ have the same relations. For each composition, the concentration of each monomer ($[A]_{Measured}$ or $[B]_{Measured}$) is known from the UV measurement. The fraction of competent protein that participates in the interaction and the fraction of incompetent protein was determined through fitting. Iterative nonlinear curve fitting in the Calypso software (Wyatt Technology) was used to determine the monomer molar mass and K_{ij} for each complex formed. Calypso uses the Levenberg-Marquardt algorithm for nonlinear curve fitting.

Size-exclusion column (SEC) MALS

All buffers were filtered through a 0.02-µm filter (Anodisc 47, catalog No. 6809-5002; Whatman). 100 µM CaM or 100 µM SKp-CaM complex were dialyzed against 20 mM HEPES, either 100 mM or 500 mM NaCl, and 2 mM $CaCl_2$, pH 7.0. Aliquots of samples (~20 µl) or buffer were fractionated at room temperature by a TSK-GEL G3000PW$_{XL}$ SEC (300 mm × 7.8 mm [inside diameter], 14 ml column volume; TosoHaas Bioscience LLC) before measurements at 25°C in a DAWN EOS static light-scattering instrument (Wyatt Technology) as described previously (Callaway et al., 2006; Kaoud et al., 2011). To normalize the light scattering detectors, 2.5 mg/ml of BSA monomer (A1900; Sigma-Aldrich) was also fractionated on the G3000 SEC. Chromatography was conducted at a flow rate of 0.4 ml/min at room temperature, requiring 40 min to complete the elution of the protein sample. Insoluble components were removed via centrifugation for ~30 s before injection from a 20-µl loop. Molar masses and peak concentrations were determined using Astra 4 and 5 software (Wyatt Technology). In 500 mM NaCl, CaM was used to elute SKp, which was bound to the column. When CaM removes SKp from the column, two maxima were observed when monitoring the differential refractive index, one maximum for the complex of CaM and SKp and one for excess CaM. For measuring the mean and variation of

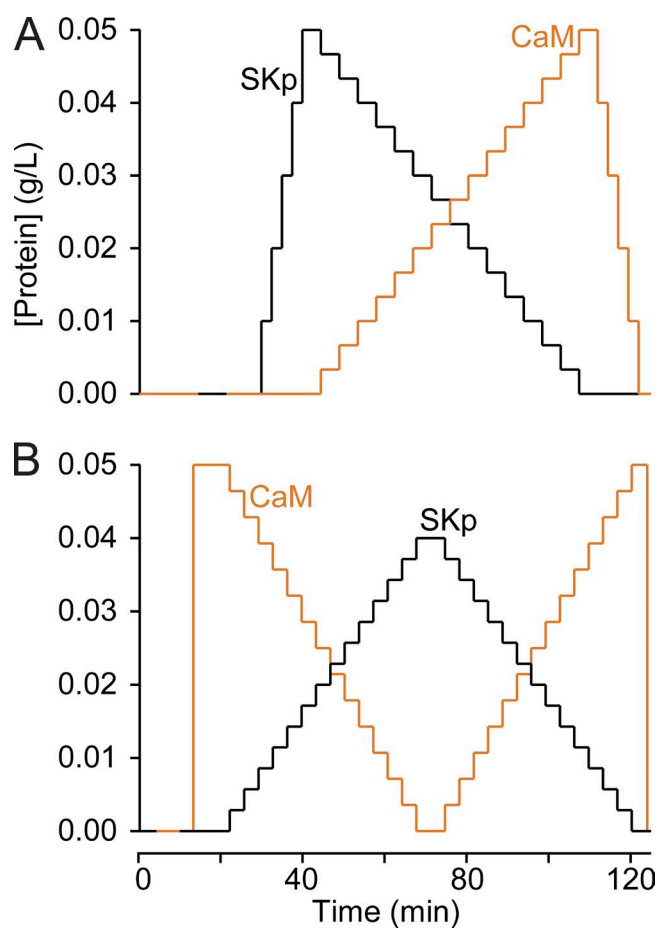

Figure 2. CG-MALS protocols. Samples are mixed just before entering the flow cell where light scattering is measured. The composition of the sample in the flow chamber over time is controlled by the following protocols: (A) Self+hetero-association protocol is used to determine the presence of homo-oligomers and hetero-oligomers. The concentration of SKp increases with steps until its maximum concentration is reached. A broad range of molar ratios of SKp:CaM are achieved by changing the composition of the mixture at each step with decreasing SKp, but increasing CaM. When SKp is zero and CaM is at its maximum, homo-association of CaM is evaluated by decreasing CaM concentration at each step. (B) Dual crossover protocol is used to evaluate hysteresis of binding. SKp concentration is shown in black and CaM concentration is shown in orange.

the measurement of mass, trials in both 100 mM NaCl and 500 mM NaCl were combined. This led to weaker but more generalizable conclusions for measurements of mass.

Solution density and sample partial specific volume

Density and specific gravity of solutions were measured on a DMA 5000 density meter at 20.001°C (Anton Paar). Proteins were dialyzed with six exchanges against 4 liters of water over three days before measurements. After measurements, solutions were weighed, dried, and reweighed on a balance (XP105DR; Mettler Toledo). Specific volume (inverse of specific gravity) was plotted against percent protein mass (weight protein/weight solution) similar to what was done with BSA (Bernhardt and Pauly, 1975), but as suggested by Lewis and Randall (1961). The partial specific volume is extrapolated at 100% protein from either a linear fit or a tangent to the curve if the data are nonlinear, but a partial specific volume is desired for a specific range of protein concentration. With the molecules we studied, the data are linear through attainable concentrations. The errors were determined by propagation of error for density measurements and mass measurements. Partial specific volume of the SKp/CaM complex was measured at each concentration with fourfold molar excess Ca^{2+}. Corrections and controls for added Ca^{2+} were applied for mass and density measurements. Measurements are included in Table 1.

Analytical ultracentrifugation

Data were collected on an analytical centrifuge instrument (XL-I; Beckman Coulter) with a two-channel epon centerpiece (Beckman or Spin Analytical) inside a rotor (AN60-Ti; Beckman Coulter). Data were collected using Data Acquisition version P4.5 (Beckman Coulter). 450-µl samples were centrifuged at 42,000 or at 55,000 rpm at 20°C. The buffers at pH 7.0 contained 100 mM NaCl, 2 mM $CaCl_2$ (saturating Ca^{2+}), or 5 mM EGTA (<5 nM or zero Ca^{2+}) and 5 mM of one of the following: Tris, HEPES, or sodium cacodylate. One experiment required adding Ca^{2+} to a total of 7 mM to obtain 2 mM free Ca^{2+} in the presence of 5 mM EGTA. Since adding Ca^{2+} to an EGTA solution releases H^+ that can drop the pH, HEPES was added to 25 mM to help stabilize the pH near 7.0. Protein concentrations varied among experiments from 15 µM to 200 µM. To obtain strong signals at different protein concentrations, different UV wavelengths were used to measure absorbance, including 230 nm, 242 nm, 280 nm, 287 nm, 290 nm, 292 nm, and 295 nm. Data were analyzed with the UltraScan III software package (UltraScan version 1.0-1206, a comprehensive data analysis software package for analytical ultracentrifugation experiments; The University of Texas Health Science Center at San Antonio, Department of Biochemistry; http:/www.ultrascan.uthscsa.edu). Time-invariant noise and meniscus position are modeled simultaneously, followed by corrected models for radial-invariant noise. The software also corrects for the density of water at 20°C. UltraScan III was used for time-derivative analysis and both van Holde-Weischet analyses and 2DSA Monte Carlo analyses. For time derivative, or dC/dt, analyses, a small subset of consecutive scans in each experiment was evaluated without removing time-invariant noise. The apparent sedimentation coefficient, s, is determined by taking the time derivative of the selected scans. The result of dC/dt is plotted as a distribution for s, which is defined as $G^*(s)$. $G^*(s)$ was normalized to the maximum value at its peak so that all data with the same molar ratio of protein could be overlaid and compared with distributions at other molar ratios. Box plots of the median, first, and third quartiles were created from the sample means. The magnitudes of the whiskers correspond to the smaller of the data range or the value of (third quartile − first quartile) × 1.5.

Van Holde-Weischet analysis (vHW) was performed for each experiment (Van Holde and Weischet, 1978; Demeler and van Holde, 2004). For statistical analysis, the integrated, binned frequencies of apparent sedimentation rates for each molar ratio were combined from all trials for comparative statistics with other molar ratios. Because the data do not show a symmetric distribution, a nonparametric permutation test was used to estimate a p-value (Pitman, 1937). The goal is to determine if the data for sample X is different from sample Y with sizes Nx and Ny, respectively. The observed means of X and Y were calculated and the difference in their means was stored. Next, test sets of size Nx and Ny were generated from random values from pooled collection of both X and Y. The means of test sets were calculated with 10,000 permutations of observed values. The difference in means of each test set was calculated, stored, and used to determine the proportion of test sets that have a greater difference in means than the observed set. If the null hypothesis is that the means of X and Y are the same, the distribution of mean differences should not depend on whether values were generated from X or Y. For example, if the experimental mean of the differences is not within 99% of the resampled sets, the null hypothesis can be rejected with a p-value of 0.01.

The same raw data were fitted by 2D spectral analysis (Cao and Demeler, 2005). Error in the fitting was estimated through 50 Monte Carlo iterations, with simulated data having similar noise distributions as the original dataset. Global fitting and Monte Carlo analysis of each sedimentation velocity dataset was performed on the UltraScan LIMS cluster operated by The University of

TABLE 1

Predicted molar mass, M, and partial specific volume, $\bar{v}$, of protein molecules or hypothetical protein complexes

Protein sample	*M* from sequence	Measured $\bar{v}$	Estimated $\bar{v}$[b]
		cm³/g (95% CI[a])	*cm³/g@20°C*
Control BSA	66.4 kD	0.743 (0.742–0.744)	0.733[c]
SKp	11.0 kD	0.726 (0.704–0.748)	
CaM	16.7 kD	0.705 (0.702–0.709)	
1SKp/1CaM[d]	27.8 kD	0.721 (0.709–0.732)	
2SKp/1CaM	38.7 kD		0.717
1SKp/2CaM	44.4 kD		0.711
2SKp/2CaM	55.4 kD		0.721[e]

[a]CI, confidence interval.
[b]Determined with UltraScan III software using Solution Management.
[c]From Sigma-Aldrich product information sheet.
[d]With 4× molar Ca^{2+}.
[e]Assuming 2/2 instead of 1/1 during measurement, $\bar{v}$ is the same.

Texas Health Science Center at San Antonio. Modeled results from a single sample can include multiple solutes, i.e., molecular species. The total concentration of all solutes combined is normalized to one. The fitted parameter, partial concentration, is plotted as contoured lines on a two-dimensional plot. The axes of the two-dimensional plot are the fitted parameters frictional ratio and either the sedimentation coefficient or molar mass. Normalized results from similar experiments were pooled and rebinned for making contour plots of combined data using IGOR Pro version 5.0.5.7 (WaveMetrics Inc.).

RESULTS

SKp binds to CaM with high affinity and can bind with different stoichiometries

A complication with the crystallographic results (Fig. 1) is that a histidine tag is present in the crystallographic studies with the SK peptide (Schumacher et al., 2001). The histidine tag in the crystallographic model (see Protein Data Bank accession no. 1G4Y) binds at the SK peptide interface and the amino acid chain of CaM that connects the N- and the C-lobes. The position of the histidine tag in the structure could complicate interpretations of both the 2/2 structure and our CaM binding measurements. A recent report suggests that the histidine tag at the interface of CaM and SK in the prior structure could have been modeled incorrectly, as a new, similar structural model more clearly shows SK residues (Zhang et al., 2013). To avoid complications we proceeded to use an SK construct without the histidine tag, which we call SKp, and purified it for binding measurements with CaM.

Although a 1SKp/1CaM complex in Ca^{2+} has not been reported to our knowledge, a 2SKp/2CaM complex was previously observed by determining structures using x-ray crystallography (Schumacher et al., 2001; Zhang et al., 2012a,b, 2013). Our initial goal was to

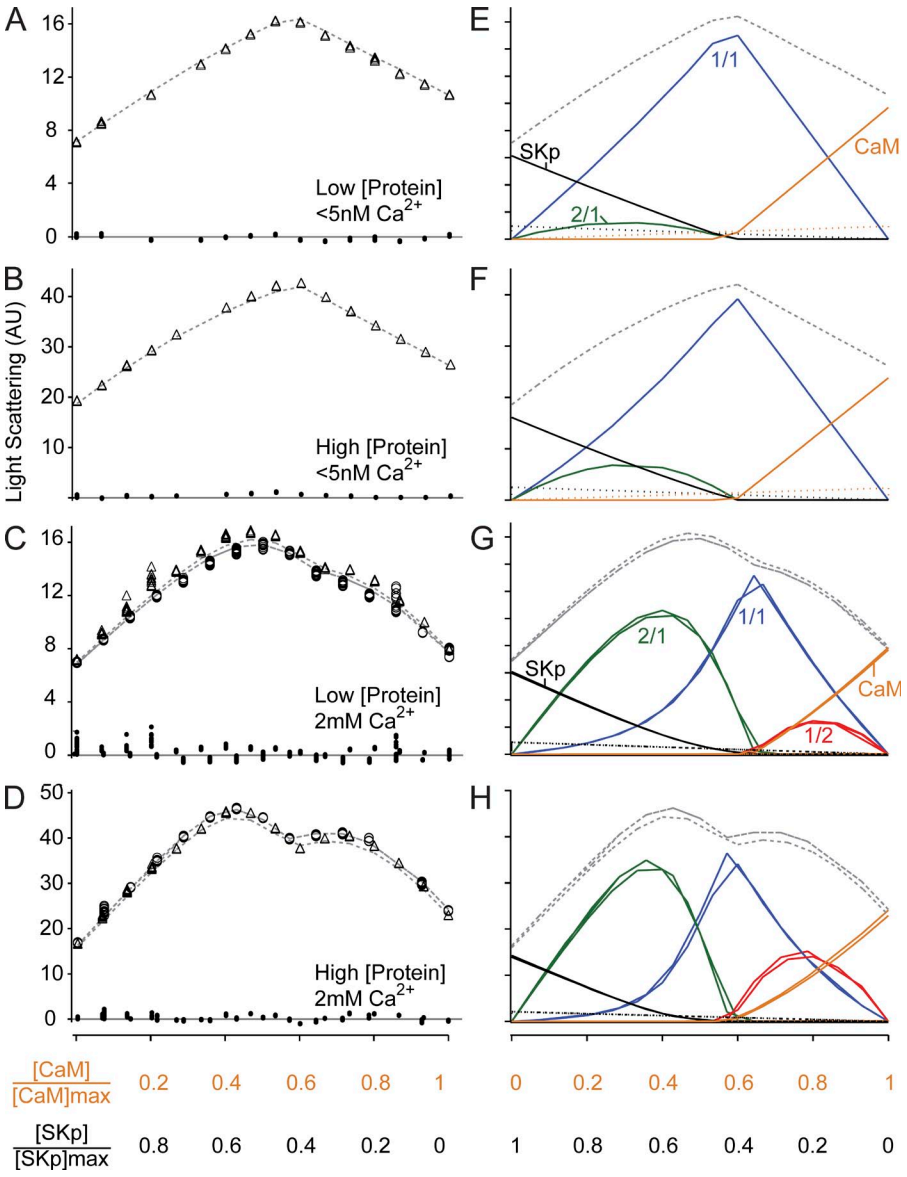

Figure 3. CG-MALS for SKp and CaM. (A–D) Black symbols show the time-averaged light scattering signal from multiple detectors as plotted versus protein composition. The composition varies with the increasing fraction of CaM (orange horizontal scale) and the decreasing fraction of SKp (black horizontal scale). Data in A and B are experiments in zero Ca^{2+} from the self+hetero-association protocol (triangles). Data in C and D are at saturating Ca^{2+} from both self+hetero-association (triangles) and dual crossover experiments (circles). All experiments in A and B were fitted simultaneously. The fits are represented by the gray broken lines. The maximum concentrations of CaM and SKp are 1.3 μM and 1.6 μM, respectively, in A for "low protein concentration," and 2.7 μM and 4.2 μM, respectively, in B for "high protein concentration." Data in C and D were also fit simultaneously. The maximum concentrations are 0.8 μM CaM and 1.6 μM SKp in C and 2.6 μM CaM and 3.8 μM SKp in D. The black closed circles distributed around the solid gray lines are the residuals to the fits. (E–H) The modeled contributions of each molecular species to the light scattering signal in A–D, respectively; the fitted curves are reproduced as broken gray lines and the vertical and horizontal axes are the same as in A–D. In E and F, the modeled contribution of each molecule to the light scattering curves are: SKp, solid black; CaM, solid orange; 2SKp/1CaM, green; 1SKp/1CaM, blue; incompetent SKp, broken black; incompetent CaM, broken orange. In G and H, the components are the same, but required the addition of a 1SKp/2CaM (red) component.

determine the stoichiometry of CaM with SKp in Ca^{2+} saturating solutions to compare with the complex that forms in a crystal environment. Table 1 lists the molar masses of both CaM and SKp, and the predicted molar masses of possible complexes that could form between the two proteins. Throughout this paper, the forward slash symbol (/) is used to describe the stoichiometry of a complex formed from multiple proteins. A colon is used to describe the molar ratio of protein concentrations in a solution.

Our goal was to study SKp/CaM complexes in solution. One way to determine the Ca^{2+}-dependent stoichiometry of SKp to Cam is to measure the molar mass of the complexes that form as a function of molar ratio. CG-MALS combines precision composition gradients with a measurement of absolute molar mass from first principles; i.e., mass is not extrapolated from standards. Two protocols were followed for collecting data: self+hetero-association and dual crossover. Both protocols measure light scattering of proteins at equilibrium after mixing at different molar concentrations of SKp:CaM. The magnitude of the light scattering signal depends on the molar mass and concentrations of the molecules in solution. If complexes form, the light scattering signal will be greater than that of either of the individual proteins being titrated. If no complex forms, the light scattering signal increases relative to the weight-average signal for the individual components. This powerful method simultaneously quantifies monomer molar mass, stoichiometry, and equilibrium association constants for self- and hetero-association complexes formed in solution.

We used CG-MALS to measure the complexes that form between SKp and CaM at zero and at saturating Ca^{2+} (Fig. 3). We define zero Ca^{2+} as <5 nM Ca^{2+} in the presence of 5 mM EGTA, and saturating Ca^{2+} as 2 mM Ca^{2+}. In Fig. 3 (A and B), light scattering signals are plotted at zero Ca^{2+}, but at different protein concentrations. Fig. 3 (C and D) likewise shows the corresponding experiments at saturating Ca^{2+}. A simple relation is shown for complex formation between SKp and CaM at zero Ca^{2+}, which shows a single peak that has a maximum signal close to where SKp and CaM are equimolar (Fig. 3 A).

At saturating Ca^{2+}, but low protein concentrations (Fig. 3 C), a maximum occurs at concentrations where [SKp] > [CaM]. There is also a shoulder where [CaM] > [SKp], which indicates formation of at least one additional stoichiometric complex. At higher protein concentrations (Fig. 3 D), there is a clear minimum between two separate peaks. A dip in amplitude is not expected for simple 1/1 interactions between two proteins.

The light scattering signal at each molar ratio of SKp:CaM depends on the contributions of each molecule or complex present in solution. We attempted to fit all of the data in Fig. 3 (A and B) simultaneously using different stoichiometric models for binding. The adjustable parameters in fitting include the following: the molar masses of SKp and CaM, percentage of SKp or CaM that is "incompetent," the concentrations of each allowed stoichiometry in a model, and the K_d for the formation of each species. Incompetent protein is defined as protein in solution that does not participate in the interaction, i.e., that is inactive, chemically modified, or misfolded. The incompetent protein fraction of either molecule is usually ~10% (Tables 2 and 3). Although not tested, incompetent protein may represent an effect from SKp gluconoylation (see mass spectrometry in Materials and methods).

In Fig. 3 (E–H), the modeled light scattering contributions of each competent and incompetent molecule, and each complex, are shown. A simple 1/1 model for a 1SKp/1CaM complex (or 2/2) with no other stoichiometries would obviously fail to fit in all conditions because it does not account for more than one peak, nor can an exclusive 1/1 model account for shoulders. Fewer stoichiometries can be resolved at zero Ca^{2+} than at saturating Ca^{2+} because there are fewer features at zero Ca^{2+}. Therefore, there are multiple possibilities that could adequately explain the zero Ca^{2+} data. In all cases, both a 1SKp/1CaM and a 2SKp/1CaM complex were needed to suitably fit the data; however, other situations

TABLE 2

CG-MALS, globally fitted parameters at zero Ca^{2+}

Sample	Molar mass[a]	Fitted incompetent fraction[b]	Fitted log (K_A)	Binding site K_d
	kD		*log (1/M)*	*nM*
SKp	11.4 (11.3–11.5)	0.153 (0.11–0.25)		
CaM	16.7 (16.5–16.9)	0.082 (0.01–0.18)		
(SKp) (CaM)	28.1		9.26 (7.3–10.1)	0.6 (0.08–2.8)
$(SKp)_2$(CaM)	39.5		14.4 (12.2–15.8)	8,000 (5,000–12,000)

Parameters are determined from globally fitted data; however, values in parenthesis are ranges of parameters determined from fitted subsets of data. The ranges were determined by floating or fixing SKp and CaM molar masses, allowing for various fitted incompetent fractions, and adding additional stoichiometries, e.g., 1SKp/2CaM complex or 2SKp/2CaM complex. The χ^2 values from fitting subsets of data or global data ranged from $0.02 < \chi^2 < 0.1$.

[a]The molar masses of SKp and CaM were fitted and the masses of protein complexes were computed by summation.

[b]Because data in this table are not tightly constrained, solutions were ignored that result in >30% incompetent fraction yield based on empirical observations that we do not have a large population of inactive protein.

provided fits that were indistinguishable from the simplest case. In one example we included a 2SKp/2CaM complex in the model for fitting at zero Ca^{2+}, but only an insubstantial fraction of 2SKp/2CaM complex was compatible with acceptable fits to the data, i.e., the maximum contribution is <5% of the light scattering signal. Acceptable fits could also be obtained with unacceptably large fractions of incompetent CaM and SKp, with >50% incompetent protein. Therefore, we present the simplest solutions with the best fit.

The light scattering signal at zero Ca^{2+} has at least two components, as shown by the modeled contributions of individual species to the light scattering fit (Fig. 3, E and F). Because other stoichiometries have larger masses and because larger masses produce more scattering, most SKp and CaM must be combined as 1SKp/1CaM to produce the observed light scattering signal. The calculated (see Materials and methods) relative mole fractions of each molecular species giving rise to the light scattering signals are shown in Fig. 4 (A–D). Virtually all of the SKp and CaM molecules are bound in a 1/1 complex at equimolar concentrations (Fig. 4, A and B). The 1SKp/1CaM complex accounts for 80% of the protein in the solution, whereas the unbound or "incompetent" SKp and CaM proteins account for the other 20%. The estimated K_d for the 1SKp/1CaM complex is <1 nM in zero Ca^{2+} (Table 2). The affinity is strong enough that the protein concentrations of SKp and CaM in this experiment have little effect on the amplitude of the mole fraction of 1SKp/1CaM. In Fig. 4 (A and B), 80% of protein is complexed at a 1SKp:1CaM molar ratio regardless of concentration used.

Although the 1SKp/1CaM complex is the dominant species at equimolar ratios, there is another stoichiometry that must be included during fitting at zero Ca^{2+}. When a 2SKp/1CaM complex is included in the model for fitting, the fits converge to the data (Fig. 3, A and B). There is a noticeable contribution from the 2SKp/1CaM complex to light scattering at zero Ca^{2+}, but the contribution is much smaller than that of the 1SKp/1CaM complex (Fig. 3 E). Its contribution is noticeably greater when the concentrations of SKp and CaM are higher (Fig. 3 F). Only a small fraction of 2SKp/1CaM in the solution relative to the 1SKp/1CaM is needed to affect the light scattering signal (Fig. 4, A and B). The apparent affinity for formation of the 2SKp/1CaM complex is weaker than 8 μM (Table 2). The data do not support the addition of other stoichiometries to improve fitting to the data.

At saturating Ca^{2+}, only multiple stoichiometries with strong affinities are compatible with the data. Similar to what is observed at zero Ca^{2+}, when the concentrations of SKp and CaM are nearly equal, nearly 80% of the protein forms a 1SKp/1CaM complex with a K_d < 100 pM (Fig. 4, C and D; and Table 3). However, if the molar ratio is not 1:1, other complexes form. When [SKp] > [CaM], a 2SKp/1CaM complex dominates the light scattering signal (Fig. 3, G and H). There is also more 2SKp/1CaM than 1SKp/1CaM in the solution when the molarity of SKp > CaM (Fig. 4, C and D). Because the K_d is ~200 nM for the 2SKp/1CaM complex, it is >10-fold stronger at saturating Ca^{2+} than at zero Ca^{2+} (Tables 2 and 3).

In addition, a 1SKp/2CaM molecule must be included to account for the second hump at higher CaM ratios (Fig. 3 D). An attempt to include the 1SKp/2CaM complex in a fit at zero Ca^{2+} produces a zero contribution, so this is strictly a phenomenon observed at saturating Ca^{2+}. Although the 1SKp/2CaM complex is larger than the 2SKp/1CaM complex (see Table 1 for predicted masses), the signal is considerably weaker (Fig. 3, G and H). This implies a lower affinity to add a second CaM to the 1SKp/1CaM complex. The modeled affinity to bind the second CaM is ~2 μM (Table 3). In Fig. 4 C, 2SKp/1CaM accounts for 26% of the protein when SKp is in excess, but 1SKp/2CaM only accounts for 6% of the protein when CaM is in excess. When proteins are injected at higher concentrations (Fig. 4 D),

TABLE 3

CG-MALS, globally fitted parameters at saturating Ca^{2+}

Sample	Fitted molar mass[a]	Fitted incompetent fraction[b]	Fitted log (K_A)	Binding site K_d
	kD		*log (1/M)*	*nM*
SKp	11.5 (11.2–11.5)	0.130 (0–0.13)		
CaM	16.4 (16.4–16.6)	0.101 (0–0.10)		
(SKp) (CaM)	27.9		10.2 (9.9–10.9)	0.06 (0.01–0.13)
$(SKp)_2$(CaM)	39.4		16.9 (16.3–17.6)	194 (190–360)
(SKp) $(CaM)_2$	44.3		16.0 (15.5–16.5)	1,750 (1,700–2,800)

Parameters were determined from globally fitted data; however, values in parenthesis are ranges of parameters determined from fitted subsets of data. The ranges were determined by floating or fixing SKp and CaM molar masses, allowing for various fitted incompetent fractions, and adding additional stoichiometries, e.g., 2SKp/2CaM complex. The χ^2 values from fitting subsets of data or global data are $\chi^2 < 0.9$.

[a]The molar masses of SKp and CaM were fitted and the masses of protein complexes were computed by summation.

[b]To show that solutions in this table are tightly constrained, some fits were performed with incompetent fractions fixed at zero, which only slightly broadened the ranges of the other parameters.

2SKp/1CaM can reach nearly 40% of the total protein when SKp is in excess, whereas 1SKp/2CaM approaches 15% when CaM is in excess.

We converted the data in Fig. 3 (A–D) to apparent molar mass (Fig. 4, E–H). We plotted it as a function of the protein composition. Simulated data are compared with the measurements. The black symbols represent the measured apparent molar mass of complexes that may form from SKp and CaM. At the maximum concentration of SKp, there is no CaM in the solution. The measured mass is equal to the mass of free SKp (Fig. 5). Assuming no interaction, as the CaM concentration increases and the SKp concentration decreases the apparent molar mass would follow a straight line representing the weight-average of the two monomers (Fig. 4, E–H). At maximal CaM concentration, the molar mass is equal to the molar mass of free CaM (Fig. 5). The simulations represent what data would look like if 100% of the molecules formed a particular complex. The simulations were generated with the following numerical guides: the maximum concentration of each protein in the simulation is equal to the maximum concentration of each protein during the experiment, and each simulation uses subnanomolar affinities for the formation of each complex to get the maximum height possible if a complex were to form. Lower affinity interactions produce peaks that do not approach the actual molar mass of the presumed complex. The blue traces in the simulations show that if 100% of the protein forms a 1SKp/1CaM complex, the maximum occurs where the molar ratio of SKp and CaM is equal to one. The height of this peak is equal to the 1SKp/1CaM molar mass for a high-affinity site.

In Fig. 4 (E and F), the maximum apparent molar mass at zero Ca^{2+} is very close to the actual mass of a 1SKp/1CaM complex. Thus any larger stoichiometries, such as a 2SKp/2CaM complex, must be substantially lower in concentration. In Fig. 4 (G and H), at saturating

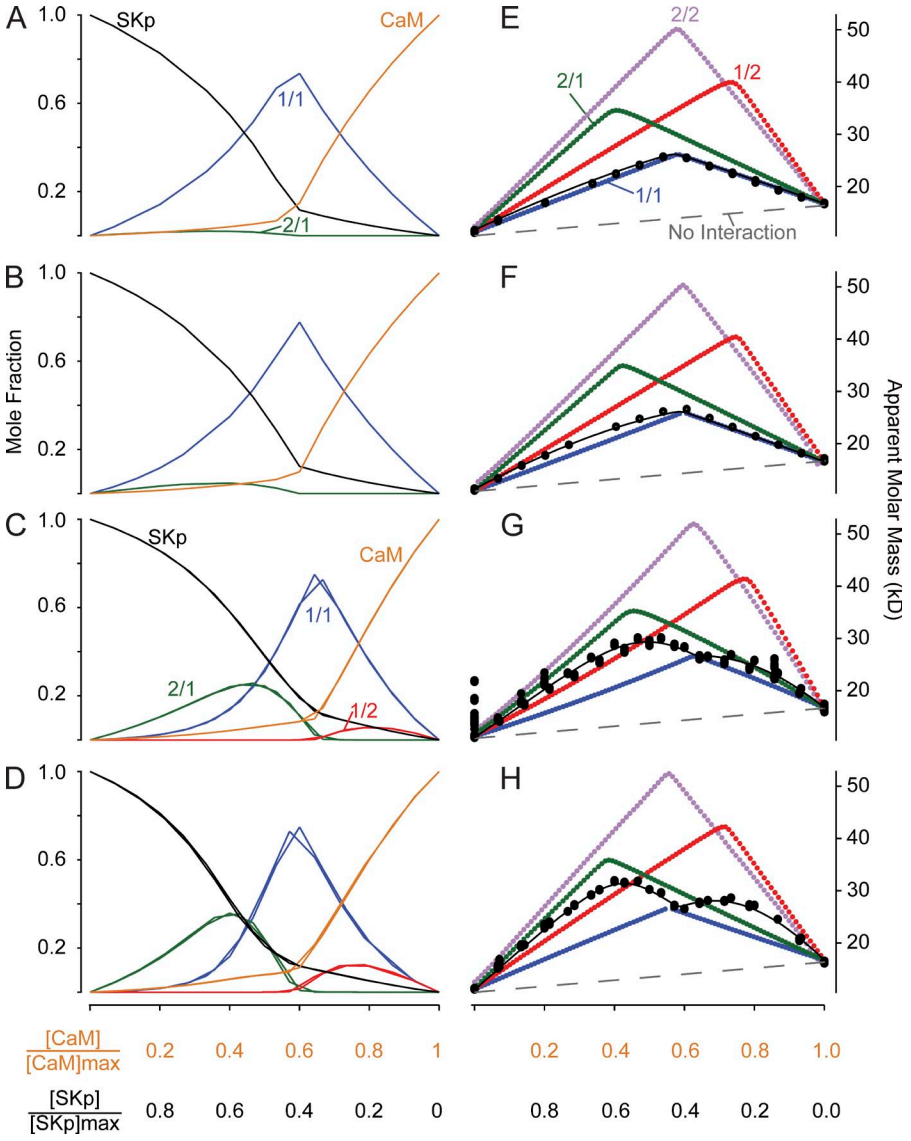

Figure 4. Mole fraction calculation and apparent molar mass simulations from CG-MALS data. (A–D) The mole fraction of each molecular species determined from the fits in Fig. 3 (A–D, respectively). As such, protein concentrations and Ca^{2+} levels in each panel correspond to A–D in Fig. 3. (E–H) Apparent molar mass plotted against the fraction of protein in solution. Black symbols in E–H are apparent molar masses that were calculated directly from Fig. 3 (A–D, respectively). Simulation curves are shown as dotted lines. The heights of the simulated curves depend on the molar masses of the proteins in the mixture, the macroscopic equilibrium constant, and the protein concentrations. The dotted lines are simulations that assume 100% of the SKp/CaM protein is bound as 2/2 complex (lavender), 2/1 complex (green), 1/2 complex (red), 1/1 complex (blue), or no interaction (gray). The simulations shown as solid black traces assume the following: two complexes, i.e., the 1/1 and 2/1, form at zero Ca^{2+} in E and F; three complexes, i.e., the 1/1, 1/2, and 2/1, form at saturating Ca^{2+} in G and H. The simulated dissociation constants are the same values that were determined from the fits in Tables 2 and 3. The incompetent protein fraction was also included as part of the simulation. The apparent molar mass of a molecular complex approaches the predicted molar mass if the concentrations of each protein are sufficiently greater than the macroscopic equilibrium constant.

Ca^{2+} a dip in the amplitude of the data points is observed at 1:1 molar protein concentrations. The apparent molar mass is equal to the theoretical molar mass of the 1SKp/1CaM complex. This essentially excludes any possibility of a 2SKp/2CaM complex forming in solution, or else the apparent molar mass would not be smaller at 1:1 molar ratios than at other molar ratios. This is especially true because both 2SKp/1CaM and 1SKp/2CaM exist. Without a high-affinity 1SKp/1CaM complex, the apparent molar mass would be influenced by both larger stoichiometries and would "flatten out" the apparent molar mass as the composition changes from excess SKp to excess CaM.

The green simulated curves (Fig. 4) also show that if 100% of the proteins form a 2SKp/1CaM complex, the maximum apparent molar mass is expected to be smaller than if 100% of the proteins form a high-affinity 1SKp/2CaM complex shown in red, because a 1SKp/2CaM complex has a larger molar mass. The maximum height in the measured data approaches the molar mass of the 2SKp/1CaM complex when [SKp] > [CaM]. The smaller bump in the titration series occurs where [SKp] < [CaM]; however, the apparent molar mass is smaller than at high molar ratios of SKp. This is because there is less 1SKp/2CaM in solution than 1SKp/1CaM (Fig. 4, C and D) so the weight-averaged molar mass is smaller, which is also indicative of a weaker affinity to form 1SKp/2CaM.

A model for apparent molar mass was simulated using the fitted K_d parameters in Tables 2 and 3. The simulation is shown as solid black lines in Fig. 4 (E–H). The simulated curves overlap the measured data. Our data support the formation of two stoichiometries at zero Ca^{2+}, but three stoichiometries at saturating Ca^{2+}. In the presence or absence of Ca^{2+}, we find no evidence of the 2SKp/2CaM complex suggested by prior crystal structures. The most striking difference between the data at zero Ca^{2+} and at saturating Ca^{2+} is the absence of the 1SKp/2CaM complex. This is the first clear evidence that Ca^{2+} drives changes in stoichiometry between SKp and CaM.

Concentration gradients of a protein without a partner are performed at the beginning and end of self+hetero-association experiments (Fig. 2). These data provide more detail into how the complexes form. For example, one CaM molecule may bind to a dimer of SKp molecules, or a 1SKp/1CaM complex may need to form before a second SKp molecule can bind. If proteins self-oligomerize, measuring the concentration dependence of apparent molar mass of a protein without partner will provide evidence for self-association. Fig. 5 shows that across the concentrations used for CG-MALS, neither SKp nor CaM form homo-oligomers. Furthermore, Tables 2 and 3 show that the fitted molar masses for SKp and CaM are very close to their predicted values in Table 1. The lack of homo-oligomerization, and the very strong affinity of SKp for CaM, suggests that the different stoichiometries are not formed by a partner binding to a homodimer.

One disadvantage of CG-MALS is that it is performed in batch mode. Size-exclusion chromatography combined with light scattering (SEC-MALS) resolves species of molecules before entering the light scattering flow cell (Slotboom et al., 2008). In addition, because CG-MALS was performed at low protein concentrations (<5 µM) that could have missed evidence of other weaker oligomers, we measured the mass of the complex that SKp forms with CaM at up to 100-µM protein concentrations by SEC-MALS. First, CaM was applied to a molecular-sieve column in the MALS system to measure light scattering and differential refractive index. In Fig. 6 (A and B), the solid curves represent the protein signal from the refractometer. The circles are the real-time measurements of the molar masses of proteins after size fractionation. CaM elutes from the column at 6.85 ml. Data from the entire peak were analyzed to obtain the weight-average molecular weight (Zhu et al., 1996; Kaoud et al., 2011). These papers show that band broadening is best used for single component samples. We don't use band broadening because it conceals components that elute close together. The entire peak is required because of the spreading of the peak between the light-scattering photometer and the refractometer (Zhu et al., 1996; Callaway et al., 2006). CaM (34 µg) was injected, and the in-line refractometer measured 29 µg of protein, with the differential index of refraction (dn/dc) assumed to be 0.185 ml/g (Barer and Joseph, 1954). After averaging $n = 4$ trials, the calculated weight-average mass of CaM was 17.7 ± 1.3 kD (Fig. 6 A), close to the predicted value of 16.9 kD based on the amino acid sequence (see Table 1). We next incubated an equimolar (100 µM) mixture of CaM and SKp in

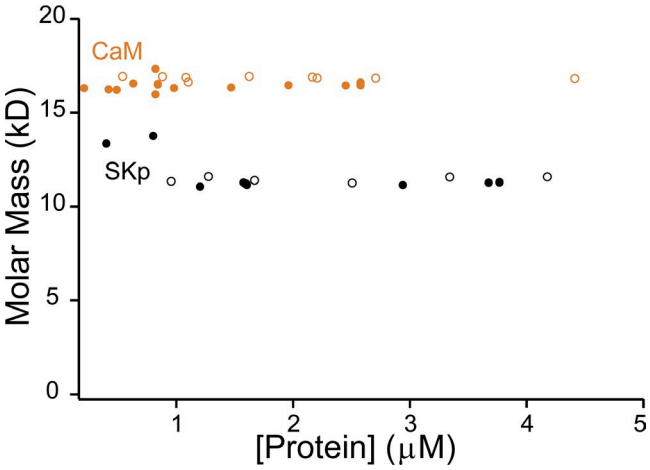

Figure 5. The protein concentration dependence of molar masses of free SKp and CaM determined from the self+hetero-association protocol measured at high Ca^{2+} (closed circles) or zero Ca^{2+} (open circles). Data for SKp are black symbols; CaM data are shown with orange symbols.

2 mM Ca^{2+} for 24 h before the complex was injected onto the SEC. Protein elution is detected at 6.85 ml, the same volume at which free CaM elutes. However, the measured weight-average mass of this mixture is 27.7 ± 2.9 kD with $n = 3$ trials (Fig. 6 A); this is consistent with a 1:1 stoichiometry, which has a predicted value of 28.0 kD (see Table 1). These data caution against using size-exclusion chromatography exclusively as a method for analyzing the formation of protein complexes because the protein complex elutes at the same volume as one of its parts, depending on the confirmations involved. This is not surprising because size-exclusion chromatography separates molecules based on multiple physical parameters that include hydrodynamic volume, intrinsic viscosity, and interactions with the column matrix, in addition to solute mass (Wang et al., 2010). Thus a dumbbell-shaped molecule like free CaM has the same retention volume on the G3000 SEC as the SKp/CaM complex, which may be more globular but occupies a similar hydrodynamic volume.

SKp by itself with 0.1 M NaCl in the buffer sticks to the column matrix and fails to enter the light scattering chamber. No SKp eluted when NaCl was increased to a concentration of 0.5 M in the buffer. To remove SKp from the column, 100 µM CaM in the 0.5 M NaCl and 2 mM $CaCl_2$ buffer was injected into the column. Fig. 6 B also shows that CaM is capable of displacing SKp from the column by forming a SKp/CaM complex, as demonstrated by the two peaks in the red curve. In 100 mM NaCl, CaM elutes at the same retention volume, 7.0 ml, as SKp/CaM (Fig. 6 A). In 500 mM NaCl, the CaM-SKp complex elutes at 7.05 ml, before the free CaM peak at 7.65 ml (Fig. 6 B). The molecule that elutes in the first peak in Fig. 6 B has a mass comparable to a 1SKp/1CaM complex with a mass of 28.7 kD. The second peak has a mass very close to that of unbound CaM, 18 kD. A change from 0.1 to 0.5 M NaCl has a greater effect on the elution volume (i.e., retention volume) of free CaM, which indicates that the hydrodynamic volume of CaM in solution is sensitive to salt. The main finding using MALS is that regardless of how the SKp/CaM complex journeys through the column matrix, the mass of the complex eluting from a column is consistent only with a 1/1 stoichiometry, at a 100-µM protein concentration.

In Ca^{2+}, the existence of three stoichiometries of SKp/CaM are confirmed across wide ranges of total protein concentrations in sedimentation velocity measurements, but 2SKp/2CaM is not observed

An independent approach to detecting protein complex formation is measuring sedimentation velocity in an analytical centrifuge (SV-AUC). The partial specific volumes of SKp, CaM, and 1SKp/1CaM were measured and recorded in Table 1. SV-AUC measures how a solution of particles sediments in a time-dependent manner in a centrifugal field, and the sedimentation progress is periodically observed by scanning the cell with UV light to monitor the distribution of protein concentration by its absorbance. As molecules sediment radially outward, the concentration of protein decreases at smaller radial distances, and the half-maximal absorbance moves radially outward with each successive scan. Example datasets that have been corrected for time-invariant and radial-invariant noise are shown in Fig. 7. After noise subtraction, the stochastic noise that remains is represented by the residual traces below each panel. The sedimentation of SKp and CaM at equimolar concentrations is shown in Fig. 7 A. Each scan is taken minutes apart. One experiment has up to 150 scans. Each scan has a characteristic sigmoidal shape. In contrast, there is a double sigmoid curve observed with fivefold molar excess SKp over CaM as shown in Fig. 7 B. This could be explained by protein absorbance having contributions from a faster sedimenting complex and from slower sedimenting free SKp.

We used two methods to measure the sedimentation coefficient (s) values in our experiments. As a parameter, s is quantitatively related to how fast particles can sediment normalized by acceleration. The coefficient

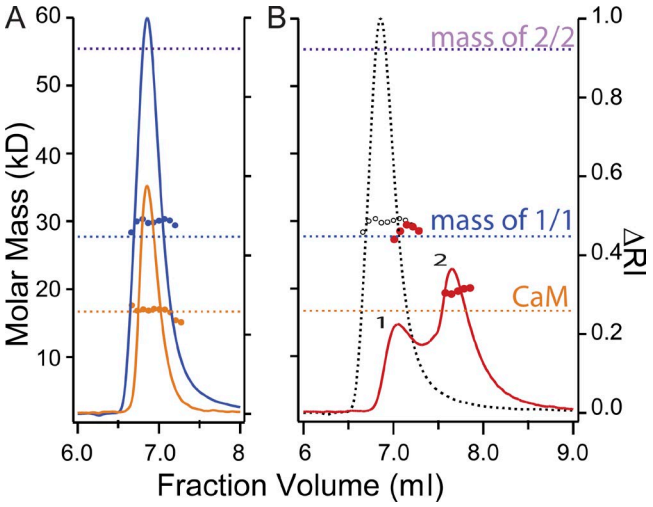

Figure 6. Determination of the molar mass by MALS. (A and B) Data for SEC-MALS. The horizontal broken lines are the predicted molar masses given by the left vertical axes for free CaM (orange broken lines), a 1/1 SKp/CaM complex (blue broken lines), and a 2/2 complex (lavender broken lines). The solid traces are the change in the differential refractive index (ΔRI scale on right vertical axis) after size-exclusion chromatography fractionation as determined by an in-line refractometer. The closed circles show the molar mass calculated from MALS. (A) 100 µM free CaM (orange data) or 100 µM molar mixture of CaM + SKp (blue data) was fractionated in a low-salt solution of 100 mM NaCl, 5 mM HEPES, and 1 mM $CaCl_2$, followed by MALS. (B) The red trace shows the elution profile of the 29 kD complex (peak 1) formed as 100 µM CaM in a buffer of 500 mM NaCl, 5 mM HEPES, and 1 mM $CaCl_2$, pH 7.0, which binds to and releases previously bound SKp from the column. Peak 2 represents free CaM. The black broken ΔRI curve and the black open circles are the same data from A for the SKp/CaM complex in low salt.

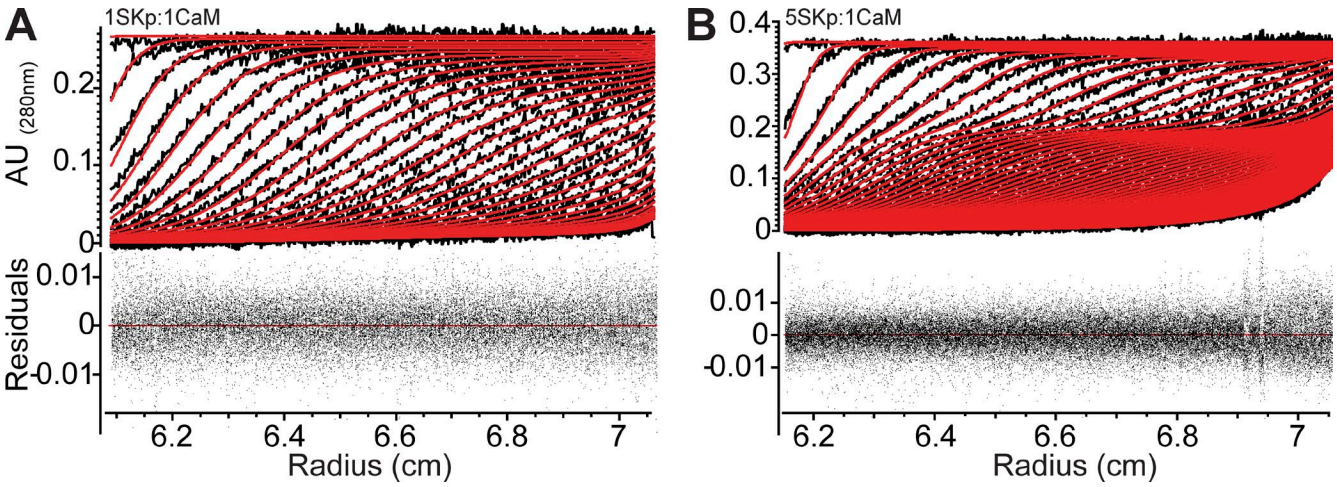

Figure 7. Representative subset of sedimentation velocity data. Data are shown as black traces with time-invariant and radial-invariant noise subtracted from raw data. Molar ratios of the proteins from representative experiments are 1SKp:1CaM (A) and 5SKp:1CaM (B). For clarity, every fifth scan is shown. The models for noise correction are shown as red lines and were determined using UltraScan III software. The bottom panels show residuals representing stochastic noise.

has a unit of time, e.g., seconds. Particles that sediment faster will have a greater value for *s*. One way to quantify the sedimentation is by taking the time derivative of the concentration profile, dC/dt (Stafford, 1992). This type of analysis has the advantage in that measurements are not influenced by small to moderate amounts of time invariant noise. Also, because the measurement is largely a derivative of a set of scans, the calculated parameters are not heavily model dependent. One major weakness is that diffusion is not accounted for, but diffusion can affect the measurement of *s*, especially for slowly sedimenting molecules (Schuck, 2000). In brief, dC/dt is

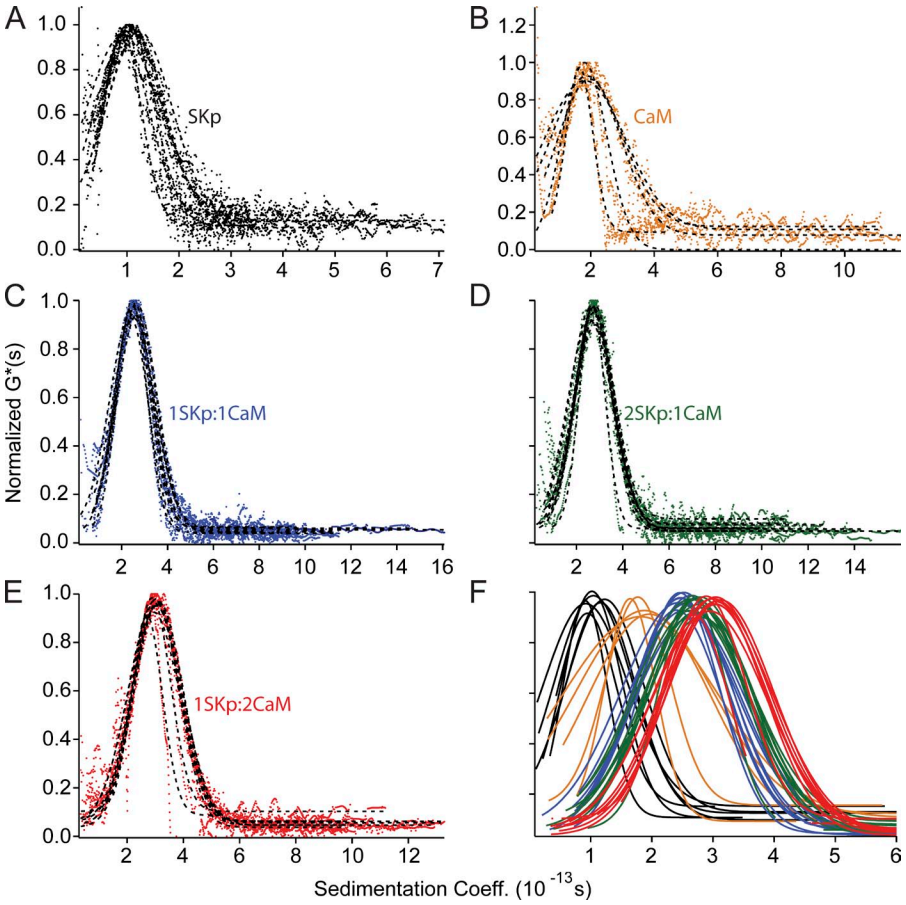

Figure 8. Time-derivative analyses of velocity data in 2 mM Ca^{2+} determined by dC/dt analysis in the UltraScan III software. (A–E) The data show normalized sedimentation coefficient distributions. Several experiments at different total concentrations, but at the same molar ratio, are plotted on the same graph. Individual experiments were fitted with Gaussian curves, represented as black broken lines. (A) SKp, black circles. (B) CaM, orange circles. (C) 1SKp:1CaM, blue circles. (D) 2SKp:1CaM, green circles. (E) 1SKp:2CaM, red circles. (F) Fitted lines from A–E plotted together for comparing sedimentation behavior at different molar ratios on same axes.

performed on a small subset of sequential absorbance scans, which are selected to have no interference from the meniscus and have a stable protein absorbance plateau at larger radii. Fig. 8 shows distributions of apparent sedimentation coefficients calculated from dC/dt. Normalizing the distributions to the peak value allows one to compare experimental trials or conditions.

vHW (Van Holde and Weischet, 1978) is capable of determining the sedimentation coefficient without the need for intensive modeling or correcting for the contribution from diffusion. A subset of the scans from data, such as those in Fig. 7, are chosen to include only the data that have a stable absorbance plateau and are far removed from the meniscus. The absorbance axis of each dataset is divided into evenly distributed boundaries, and each boundary line crosses all of the scans, but intersects each scan only at one radial position. The distance between scans along a boundary shows net molecule displacement over time. The time displacements along a boundary are extrapolated to infinite time to provide a measurement for the sedimentation coefficient, *s*, for that boundary. The extrapolated *s* for each of 110 boundaries is plotted in Fig. 9 A, and plots are shown for each experiment. This type of plot can provide information on whether there is sample heterogeneity or nonideality. Heterogeneity of samples or samples with nonideality would produce a broad distribution of *s* values. Alternatively, *s* of homogeneous samples are confined to a nearly vertical line (Van Holde and Weischet, 1978). In Fig. 9 A, all samples appear mostly homogeneous, i.e., the distribution of *s* values is almost vertical. There are some scans where *s* increases toward the upper boundaries, which suggests that small amounts of oligomers or aggregates form. Drawing a vertical line through the data gives a good estimation of *s*.

Both dC/dt and vHW provide consistent measures for the molecular sedimentation. The mean sedimentation coefficients, *s*, are listed in Table 4 and shown in Fig. 11. The measured *s* for SKp is $\sim 1.0 \times 10^{-13}$ s, and this is easily resolved by eye in Figs. 8 A and 9 A. Even with different centrifuge speeds and different total protein concentrations, there was little difference in the measured mean, although there was some variability in the width of the dC/dt distributions (Fig. 8 A). We note that one noisy outlier was removed from these analyses because of an insufficient number of scans.

CaM, a larger molecule, migrates faster with a coefficient near 2.0×10^{-13} s (Figs. 8 B and 9 A). Of the conditions we studied, the sedimentation profile of CaM seems the most sensitive to rotor speed. In Fig. 8 B, higher rotor speeds accounted for the narrower distributions, but this is partly expected as diffusion has a smaller effect at faster speeds.

When SKp is combined with equimolar CaM to form a complex, a molecule with $s = 2.5 \times 10^{-13}$ s is formed (Figs. 8 C and 9 A). The change in sedimentation of CaM in the presence of SKp strongly suggests the formation of a complex, which is consistent with light scattering data. For a more complete analysis using vHW, several datasets with the same protein composition were combined and the *s* values were binned so that the integrated frequency of *s* measurements could be plotted in

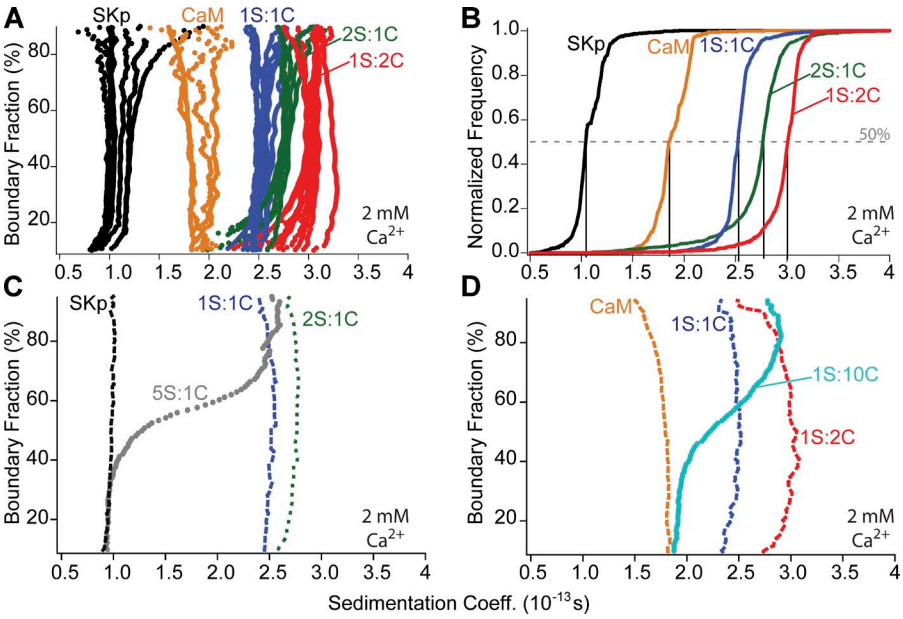

Figure 9. vHW analyses of sedimentation velocity data in saturating Ca^{2+}. (A) Multiple experimental trials in the presence of 2 mM Ca^{2+} were analyzed by the vHW method. Scans like Fig. 7 are divided into boundaries that cross all scans in a dataset, and the sedimentation coefficient, *s*, from each boundary is extrapolated at infinite time; the *s* for each boundary is plotted on this graph. From left to right: black, SKp; orange, CaM; blue, molar ratio 1SKp:1CaM; green, 2SKp:1CaM; red, 1SKp:2CaM. (B) Integrated data from several experiments with the same color coding as in A. All the *s* values from an experiment were binned, combined with other data that have the same molar ratio of protein, and normalized to the maximum number of observations for a particular s. The data are plotted as normalized frequency versus *s*. The s_{50} is determined by the intersection of each integrated curve with the horizontal (gray broken line), which represents 50% of total data from a sample set. Vertical drop lines are included to facilitate estimation of s_{50} by eye. (C) Representative data from A are shown as broken lines: SKp, black; 1SKp:1CaM, blue; 2SKp:1CaM, green. The gray symbols show a result for 5SKp:1CaM at saturating Ca^{2+}. (D) Representative data from A are shown as broken lines: CaM, orange; 1SKp:1CaM, blue; 1SKp:2CaM, red. The cyan symbols show a result for 1SKp:10CaM at saturating Ca^{2+}.

TABLE 4

Sedimentation coefficient, s, determined from vHW

Sample	Zero (EGTA) or saturating Ca^{2+}	*n* trials	$s \pm SD^a$ (vHW)
			10^{-13} s
Free SKp	Ca^{2+}	8	1.06 ± 0.09
Free CaM	Ca^{2+}	4	1.91 ± 0.12
1SKp:1CaM	Ca^{2+}	10	2.52 ± 0.07[b,c]
2SKp:1CaM	Ca^{2+}	8	2.76 ± 0.10[b]
1SKp:2CaM	Ca^{2+}	9	3.02 ± 0.10[c]
1SKp:1CaM (<68 μM)	EGTA	6	2.25 ± 0.10
2SKp:1CaM (<68 μM)	EGTA	6	2.09 ± 0.09
1SKp:2CaM (<68 μM)	EGTA	6	2.34 ± 0.11
1SKp:1CaM (>68 μM)	EGTA	2	2.9 ± 0.3
2SKp:1CaM (>68 μM)	EGTA	3	4.2 ± 0.4
1SKp:2CaM (>68 μM)	EGTA	3	2.48 ± 0.05

[a]SD of combined stable data points (80% total, from 10 to 90%) at t = ∞ from vHW analysis from combined trials.
[b] and [c]Nonparametric null hypothesis permutation test determination that compared samples, (i.e., b to b or c to c) are different. In both cases P < 0.0001.

Fig. 9 B. The data are normalized to show percent of total. In Fig. 9 B, the integrated *s* values show a steep rise with a half-maximum, i.e., s_{50}, at 2.51×10^{-13} s. We also combined dC/dt Gaussian fits into one graph for comparisons in Fig. 8 F. The means from all analyses are plotted in Fig. 10.

In addition to 1:1 molar ratios of SKp to CaM, other molar ratios were analyzed by sedimentation velocity. These include the molar ratios of 2SKp:1CaM and 1SKp:2CaM shown as green and red traces, respectively, in Fig. 8 (D–F) and in Fig. 9 (A and B). When molarities are different by twofold, the observed sedimentation coefficient is always greater than when SKp and CaM are at a 1:1 molar ratio, and these differences are significant ($P < 0.01$) as determined by a two-sample *t* test or a nonparametric permutation test (see Materials and methods; Table 4 and Fig. 10). The species that forms at 1SKp:2CaM sediments faster than the one that forms at 2SKp:1CaM. Because the molar mass of the 1SKp/2CaM complex is larger than 2SKp/1CaM (Table 1), its faster sedimentation can best be explained by having the larger mass, as opposed to conformation. This is explored in more depth in the next paragraph. Some data are not completely vertical, which may indicate some heterogeneity or influence by nonideality, but by and large the data appear homogeneous. The behavior is not strongly concentration dependent, as demonstrated by overlapping data from different experiments (Fig. 9, A and B).

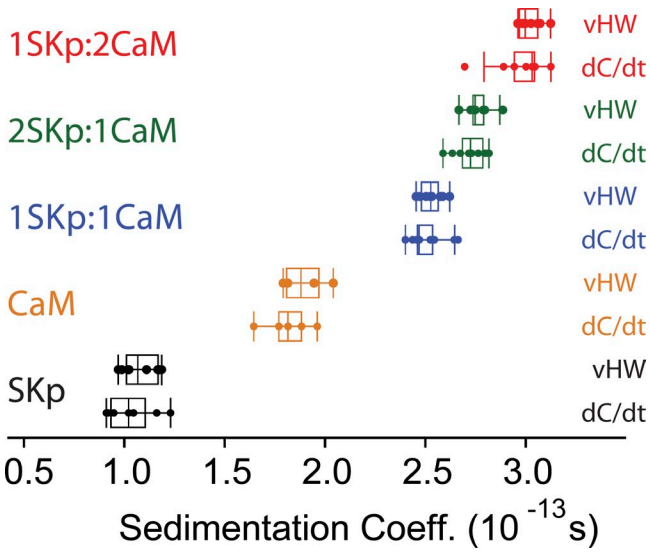

Figure 10. Summary of dC/dt and vHW data. Box plots show the median, quartiles, and ranges of sample means from all trials. A trial may be considered an outlier if it falls outside 1.5-fold the range from the first to third quartiles.

A faster sedimentation indicates a larger mass, a change in the hydrodynamic volume, or a combination of these two factors. A different stoichiometry will have a different mass. Thus further analyses of the sedimentation velocity data are needed to determine whether excess of either SKp or CaM alters either the stoichiometry or the hydrodynamic volume of the complex. Because vHW is better suited for heterogeneous experiments, dC/dt is not used for molar ratios with more than twofold differences in concentrations of SKp to CaM. When SKp is at least fivefold molar excess over CaM, the absorbance profile of the scans show two different plateau phases (Fig. 7). Applying vHW analysis clearly resolves the sedimentation coefficients of both species. Instead of vertical, the profile has one phase that aligns with the 2SKp:1CaM data and another phase that aligns with the free SKp data (Fig. 9 C). The simplest interpretation is that these phases align with a 2SKp/1CaM complex and free SKp. Similarly, when CaM is in 10-fold molar excess over SKp, vHW analysis resolves a phase that aligns with the 1SKp:2CaM data and a second phase that aligns with free CaM (Fig. 9 D). In this case, we resolve the 1SKp/2CaM and free CaM. Together, these data support our interpretations of

the CG-MALS data where both 2SKp/1CaM and 1SKp/2CaM stoichiometries were observed at saturating Ca^{2+}.

It may be possible to distinguish changes in mass (i.e., stoichiometry) or in hydrodynamic volume with sedimentation velocity data if simulated models solve for both parameters simultaneously. Although the measured values are model dependent, they can be used to distinguish qualitative changes that have occurred due to mass or shape change or both. Most of the samples that were analyzed by the vHW method were also analyzed by two-dimensional spectral analysis algorithms combined with Monte Carlo statistics, 2DSA-MC (Brookes et al., 2010). The main idea of 2DSA-MC is that the concentration of each protein solute in a solution has a different sedimentation behavior that can be uniquely measured by absorbance. The corresponding mass and hydrodynamic parameters for each solute are solved simultaneously with the partial protein concentration of each solute. This is possible because the absorbance profile depends both on the radial distribution of protein and the time at which absorbance scans across the window are collected. UltraScan III employs the use of supercomputers to search exhaustively over a large parameter space for unique solutions to the Lamm equation (Lamm, 1929),

$$\frac{\partial C}{\partial t} = k\left(\frac{\partial^2 C}{\partial x^2} + \frac{1}{x}\frac{\partial C}{\partial x}\right) - \omega^2 s\left(x\frac{\partial C}{\partial x} + 2C\right).$$

C is solute concentration at time t and at radius x, *s* is the sedimentation coefficient, ω is the angular speed of the rotor, and k is the diffusion coefficient. Plots are created that show solutions to the sedimentation velocity datasets. One useful parameter that can be fitted is the frictional ratio (f/f_o), which is proportional to the volumetric radius times the solution viscosity (Cantor and Schimmel, 1980). UltraScan III uses the Stokes-Einstein relation to relate the diffusion and sedimentation coefficients to the frictional coefficient ratio (Brookes et al., 2010):

$$f/f_o = \frac{1}{\eta}\left(\frac{RT}{k18N\pi}\sqrt{\frac{2\left(1-\bar{v}\rho\right)}{s\bar{v}}}\right)^{3/2}.$$

Here, *k* and *s* again refer to diffusion and sedimentation, R and T are the gas constant and temperature, N is Avogadro's number, η is the solvent viscosity, ρ is the solvent density, and $\bar{v}$ is the partial specific volume. The f/f_o ratio is influenced by the compactness and the hydration state of a molecule. The purpose of using f/f_o instead of the diffusion coefficient in solving the Lamm equation is that it provides the user with an intuitive guess over which range to fit the data. For example, virtually all protein shapes, except filaments, will be in the range $1 < f/f_o < 4$. A dehydrated sphere has a ratio $f/f_o = 1$ (Brookes et al., 2010). Any other value for f/f_o cannot distinguish a shape change from a change in hydration state, yet an $f/f_o > 3$ would strongly suggest a thin rod. Data in Fig. 11 are presented in terms of f/f_o versus either *s* or *M*. After first correcting for noise to get an initial model that fit a single experiment, the solutions to each trial experiment are analyzed statistically using Monte Carlo simulations to determine how broad a range of parameters can be fitted and still be within tolerance of a good fit. A contour plot helps to show these parameter ranges. Multiple experiments can then be combined and a contour plot is redrawn to represent the combined data.

The partial protein concentrations at saturating Ca^{2+} represented at a particular f/f_o and *s* are represented by contour levels in Fig. 11. An example of how the data are assembled is described in Fig. 11 A. Contour plots are generated for each trial, as shown in Fig. 11 A (inset) for equimolar SKp and CaM. All the trials for a sample are combined and rebinned to construct a contour plot of the combined data as in Fig. 11 A. Comparing different sample compositions is now possible, as shown in Fig. 11 B. As in Figs. 8 and 9, *s* is clearly resolved for SKp, CaM, and 1SKp:1CaM solutions. When equimolar SKp and CaM form a complex, the dominant density is clustered around $s = 2.5$ (Table 5). Because the *s* distribution is narrow and all other parameters are assumed, the uncertainty in f/f_o appears to be entirely caused by the implicit parameter estimation of diffusion (*k*). Diffusion is not as easily measured as sedimentation at a single rotor speed. If *k* is accepted with its uncertainty, the molar mass *M* can be determined (Brookes et al., 2010). The greatest density of observation points for 1SKp:1CaM lies at ~30 kD (Fig. 12 C). This is most consistent with a single SKp molecule binding a single CaM molecule, and there is very little experimental support for a 2SKp/2CaM complex near 55 kD. Also in Fig. 11 C and Table 5, it appears that the species that sediments with a coefficient of 2.75×10^{-13} s in 2SKp:1CaM molar ratio (green contours in Fig. 11, B and C) is more massive (~36 kD) than the species that sediments when the molar ratio is 1SKp:1CaM (blue contours at ~28 kD in Fig. 11, B and C). This suggests that an additional SKp binds to the 1SKp/1CaM complex to form a 2/1 complex when SKp is in excess. When CaM is in excess, it is less clear how to interpret the data. A peak appears within the same molecular weight range as the 1SKp/1CaM complex; however, moderate peaks are found in the ~45 kD range consistent with one additional CaM binding to the complex. Because the CG-MALS data show that the affinity for a second CaM binding to

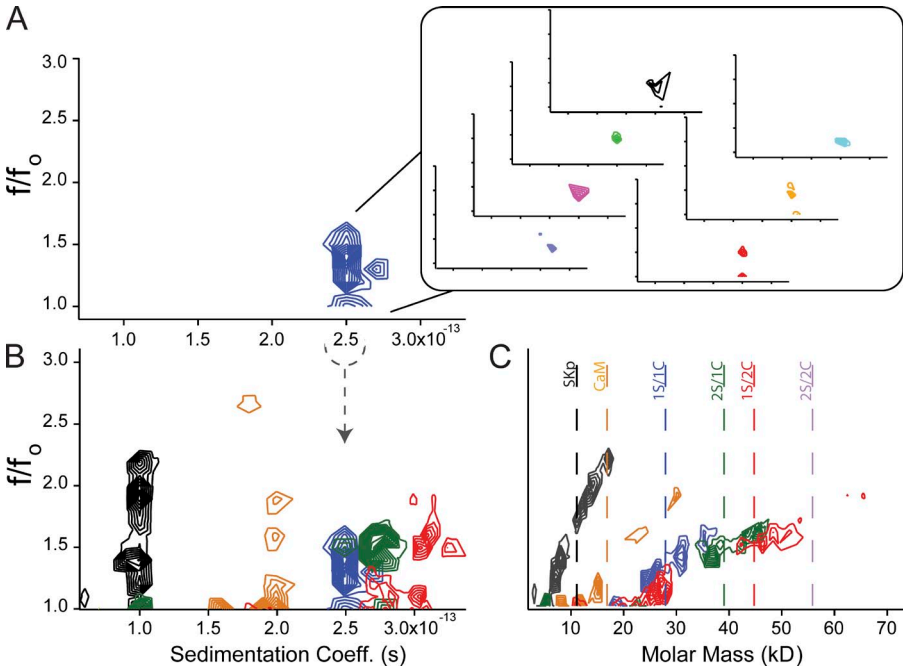

Figure 11. Contours of 2DSA Monte Carlo analyses of sedimentation velocity data. Data are plotted as the frictional ratio versus *s* (A and B) or the frictional ratio versus molar mass (C). The partial concentrations as a percentage of total protein of the modeled solutes are indicated by contoured lines. Each contour level is 10% of the relative concentration. (A) Contours of 1SKp:1CaM data. The inset shows contoured data from individual experiments drawn in different colors. Raw outputs from each experiment were combined then rebinned to produce the single contour plot (blue contours) in the main panel representing all analyzed data with 1SKp:1CaM. (B) 1SKp:1CaM data from A are compared with other samples. SKp, black contours; CaM, orange; 1:1 molar ratio of SKp to CaM, blue; 2SKp:1CaM, green; 1SKp:2CaM, red. The gray arrow is a guide to show that the 1:1 molar ratio data in B are the same in A. (C) Same as B, but the frictional ratio is plotted versus modeled molar mass. Vertical broken lines represent predicted molar masses for proteins and complexes. From left to right, the lines represent: SKp, black; CaM, orange; 1SKp/1CaM, blue; 2SKp/1CaM, green; 1SKp/2CaM, red; and 2SKp/2CaM, gray.

the 1SKp/1CaM complex is weaker (Fig. 3 and Table 3), perhaps this is a representation of both populations being present. The frictional ratio of the contours for 1SKp:2CaM that matches the molar mass of the 1SKp:1CaM data is slightly smaller. A conservative conclusion is that excess CaM influences either the conformation of the 1SKp/1CaM complex or the number of bound waters, perhaps through rapid associations.

CaM or Ca^{2+} reverses the tendency of some complexes to aggregate

Sedimentation velocity experiments were also performed at zero Ca^{2+} and analyzed by vHW. At protein concentrations up to 68 μM, varying the molar ratio of SKp:CaM has little effect on the sedimentation coefficient. In zero Ca^{2+}, the sedimentation coefficients at <68 μM protein are 2.3×10^{-13} s for 1SKp:1CaM, 2×10^{-13} s for 2SKp:1CaM, and 2.3×10^{-13} s for 1SKp:2CaM (Table 4). These values suggest that sedimentation for the 1Skp/1CaM complex is a little slower at zero Ca^{2+} than in saturating Ca^{2+}. At these protein concentrations, we were not able to resolve by SV-AUC the 2SKp/1CaM complex that was hinted at in the CG-MALS data.

Because the data in Table 2 indicate that there is a weaker affinity for 2SKp/1CaM to form at zero Ca^{2+}, we attempted sedimentation velocity at protein concentrations >100 μM. Although varying the total protein concentration at saturating Ca^{2+} had little effect on the sedimentation of any stoichiometric complex (Figs. 8 and 9), 100 μM protein uncovered a tendency toward aggregation at zero Ca^{2+} when [SKp] > [CaM] (Fig. 12 A). In Ca^{2+}, proteins in the 1SKp:2CaM sample sediment the fastest, but at zero Ca^{2+}, proteins in the 2SKp:1CaM solution sediment at a higher, but variable, coefficient of 4.2×10^{-13} s (Table 4). Integrated 1SKp:1CaM data are not vertical, which shows heterogeneity in different samples (Fig. 12 B). We may interpret this to mean that minor aggregation is still present with a 1SKp:1CaM sample, which sediments with a mean coefficient of 2.9×10^{-13} s.

TABLE 5

Calculated parameters for sedimentation coefficient, s, and molar mass, M, determined from 2D spectral analysis (2DSA)

Sample	*n* trials	*s* ± SD (2DSA)	Range of M (>80% contoured data, 2DSA)
		10^{-13} *s*	*kD*
Free SKp	7	0.95 ± 0.10	5–15
Free CaM	4	1.86 ± 0.25	8–24
1SKp:1CaM	7	2.47 ± 0.20	17–34
2SKp:1CaM	8	2.75 ± 0.10	22–47
1SKp:2CaM	9	3.01 ± 0.40	18–51

In contrast, for a molar ratio 1SKp:2CaM, the results are homogeneous within a sample, which shows a nearly vertical vHW plot, and across experiments as shown as a vertical integrated plot (Fig. 12, A and B). We measured s to be 2.5×10^{-13} s, which is approximately what we have interpreted to be the value of s for a 1SKp/1CaM complex at saturating Ca^{2+}. Because s is smaller at zero Ca^{2+} for 1SKp:2CaM solutions, this either means that the 1SKp/2CaM complex is more compact at zero Ca^{2+}, or it means that only a 1SKp/1CaM complex forms and that a second CaM molecule does not bind to the complex. Second, because there is no heterogeneity in the sample, we can conclude that aggregation is substantially reduced when CaM is in molar excess.

We measured the sedimentation over a broader range of SKp:CaM at zero Ca^{2+}. The gray curves in Fig. 12 C show data with excess SKp. With a 10-fold excess of SKp over CaM, the curve shows one phase that covers a broad range of s, and a stable phase where s is $\sim 1 \times 10^{-13}$ s, which is similar to free SKp (Fig. 12 C). This shows that not all of the SKp forms an aggregate. The aggregate only forms when CaM is present in smaller molar quantities. It appears that aggregates require multiple SKp and at least one CaM molecule. When SKp is fourfold higher than CaM, there is a mixture of dissociated SKp and aggregate (Fig. 12 C). The maximum s at fourfold excess SKp, $\sim 4 \times 10^{-13}$ s, is no greater than s observed at twofold molar excess SKp, $\sim 4.5 \times 10^{-13}$ s. Because the observation is weighted by all particles in solution, the heterogeneity may indicate that there are multiple oligomers that form in solution. We cannot resolve any oligomer or aggregate with certainty.

When the molar ratio of CaM is 10-fold higher, the maximum s is $<3 \times 10^{-13}$ s as shown in the cyan curve in Fig. 12 C. The s of free CaM is $\sim 2 \times 10^{-13}$ s, but there is no phase of the plot with excess CaM that clearly shows the sedimentation of free CaM. The vHW plot is not vertical, but slanted toward smaller s values. This finding indicates that some heterogeneity or nonideality exists during sedimentation (i.e., charge or protein concentration effect). In either case, the 1SKp:10CaM data suggests a bias toward smaller sedimentation coefficient values that are most consistent with a 1SKp/1CaM complex.

We noted that freshly thawed SKp is stable during the time course of our experiments, but after days at 4°C irreversible precipitation is observed by the eye. Only freshly thawed SKp is used in our experiments. The CG-MALS data does not show aggregation of SKp at zero or at saturating Ca^{2+} (Fig. 5). At >100 µM protein concentrations, CaM can induce precipitation of SKp that is partially reversible if [SKp] ≥ [CaM] at zero Ca^{2+}, but precipitation is not observed when [SKp] < [CaM]. This qualitative assessment suggests that excess CaM at zero Ca^{2+} prevents runaway aggregation that forms a precipitate. In contrast, at saturating Ca^{2+} no precipitation at any molar ratio of SKp:CaM is observed.

Ca^{2+} appears to have a negative effect on aggregation. Fig. 12 D shows an experiment that starts at zero Ca^{2+}. Sedimentation velocity data were collected and are shown as the open symbols. After the SV-AUC run finished, Ca^{2+} and a pH buffer was added to elevate the free Ca^{2+} to 2 mM. As a cautionary note, proteins that have sedimented at zero Ca^{2+} experience very high concentrations at the end of the centerpiece well and can precipitate out of solution. A 20–35% loss of protein was observed when comparing the runs at the maximum absorbance at time zero of each condition (unpublished data).

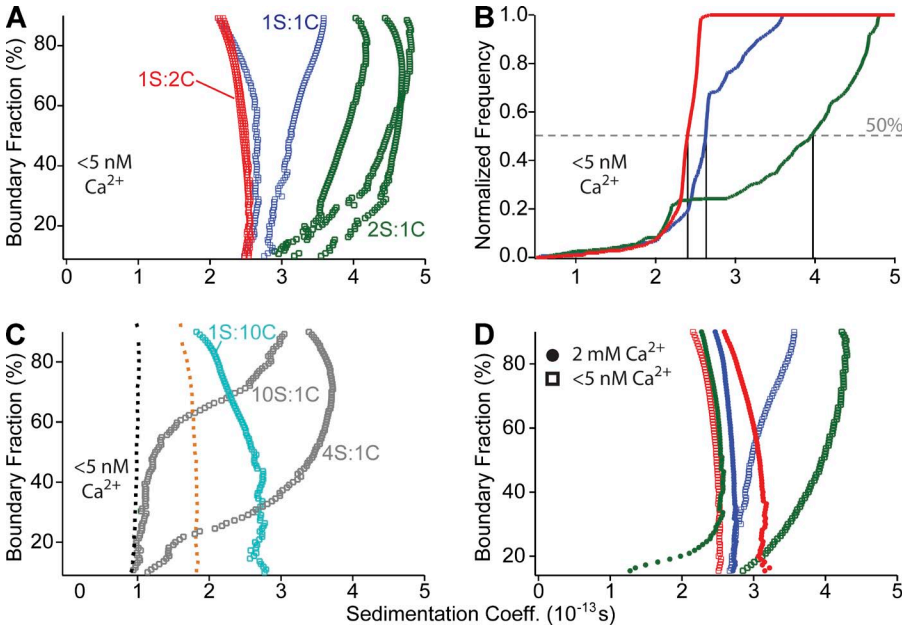

Figure 12. vHW analysis in zero Ca^{2+} shows nonideal behavior. (A) Analyses of sedimentation velocity results at zero Ca^{2+} are shown as open squares for the following solutions: 1SKp:1CaM, blue; 2SKp:1CaM, green; 1SKp:2CaM, red. (B) Integrated data in zero Ca^{2+} from data in A. (C) Open symbols show data collected at the following molar ratios: gray, 10SKp:1CaM or 4SKp:1CaM; cyan, 1SKp:10CaM. Representative traces from Fig. 9 A are shown as broken lines: SKp, black; CaM, orange. (D) Ca^{2+} reverses effects at zero Ca^{2+}. After experiments in zero Ca^{2+} (open boxes), Ca^{2+} was added to each sample and velocity data were collected again (closed circles). The following molar ratios were used: blue, 1SKp:1CaM; green, 2SKp:1CaM; red, 1SKp, 2CaM.

The open symbols in Fig. 12 D show data at zero Ca^{2+}, and the closed circles are data after Ca^{2+} was added. When comparing the curves before and after Ca^{2+} was added, proteins at 2:1 and 1:1 molar ratios of SKp:CaM have a smaller sedimentation coefficient, *s*, at saturating Ca^{2+} than at zero Ca^{2+}. Notably, the 2SKp:1CaM sample sediments much more slowly with Ca^{2+} present (Fig. 12 D). We hypothesized that the aggregates or oligomers at zero Ca^{2+} had more molecules of SKp than CaM. This would indicate a greater loss of SKp if the aggregate precipitated over the time course of the centrifugation. In fact, we did notice a reduction in the absorbance signal indicating a small loss of material. Of the material that remained, the apparent sedimentation of 2SKp:1CaM in added Ca^{2+} is comparable to or less than the observation with 1SKp:1CaM. We can conclude that Ca^{2+} reversed the oligomerization state of the proteins in the 2SKp:1CaM solution so that only a 2SKp/1CaM complex is compatible with the SV-AUC data in added Ca^{2+}.

The opposite sedimentation behavior is observed when the ratio is 1SKp:2CaM. At this ratio, *s* is greater when Ca^{2+} is added (Fig. 12 D). This shows that just adding Ca^{2+} to a 1SKp:2CaM molar solution can result in a molecular species that sediments faster.

The following conclusions can be made from Fig. 12 D: at zero Ca^{2+}, aggregation that is present in both the 1SKp:1CaM and 2SKp:1CaM is reversed with saturating Ca^{2+}, and the 1SKp:2CaM condition is the only sample that shows an increased sedimentation coefficient when Ca^{2+} is added, which is consistent with CG-MALS showing that the 1SKp/2CaM complex only forms in Ca^{2+}.

DISCUSSION

Our studies of CaM binding to SKp in solution are summarized as a scheme shown in Fig. 13. Multiple stoichiometries can form at zero and at saturating Ca^{2+}. At zero Ca^{2+} (<5 nM), SKp and CaM bind in a 1/1 complex (Fig. 13 A). In excess SKp, a second SKp may combine to form a 2SKp/1CaM complex. We presented some evidence that additional oligomeric or aggregated states can form. When Ca^{2+} saturates the complex, SKp and CaM can combine in a 1SKp/1CaM, a 2SKp/1CaM, or 1SKp/2CaM complex (Fig. 13 B). The 1SKp/2CaM complex was not observed in any experiment at zero Ca^{2+}. A 2SKp/2CaM complex observed in a crystal structure is not present in our solution studies in zero or saturating Ca^{2+} concentrations. These results are not consistent with the 2/2 gating model, where Ca^{2+} binding drives a transition from 1/1 to 2/2 complexes.

The 2/2 gating model proposes a modular role of CaM in SK activation. At low Ca^{2+}, the complex that forms is 1SK/1CaM, with only the C-lobe of CaM engaged. An increase in intracellular Ca^{2+} drives Ca^{2+} binding only to the N-lobe of CaM, and a 2SK/2CaM interaction forms. Although the 2/2 gating model is consistent with the crystallographic results for a single conformational state, there has been some physiological evidence that it is insufficient to describe channel gating. For instance, the part of CaM responsible for Ca^{2+} dependent binding, the N-terminal lobe, also has an effect on Ca^{2+}-free interactions with SK (Li et al., 2009). It is clear that our understanding of the role of CaM in SK gating is inadequate.

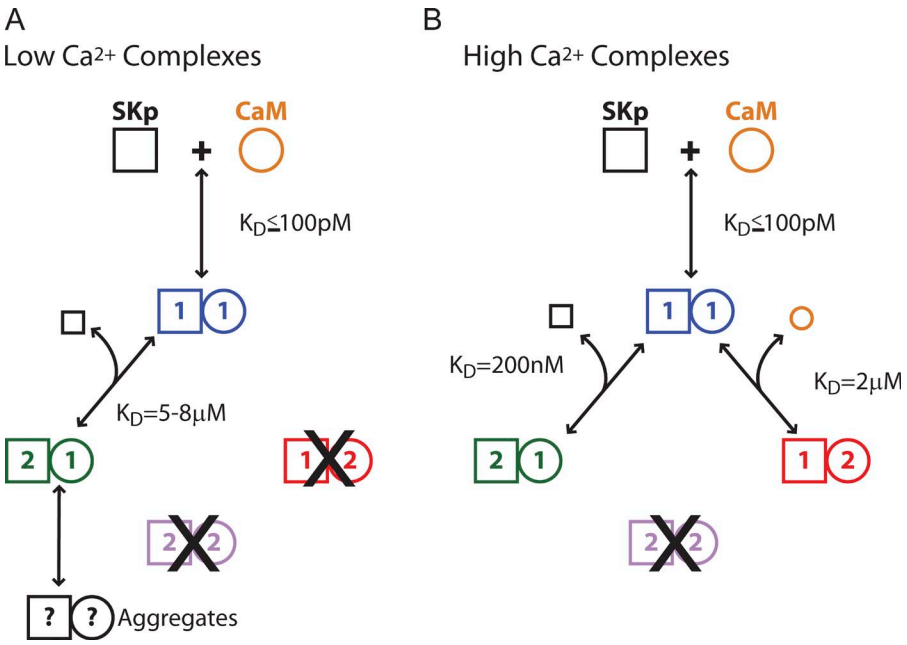

Figure 13. Scheme for observed oligomerization of SKp/CaM. Colors are consistent with the other figures. We make no claim as to the configuration of the complexes beyond the stoichiometric ratio. (A) In zero Ca^{2+}, SKp and CaM can form a 1/1 complex, a 2/1 complex, and possibly higher order oligomers or aggregates. A 1/2 oligomer was not observed. (B) In high Ca^{2+}, SKp and CaM can form a 1/1 complex, a 2/1 complex, or a 1/2 complex. Higher-order oligomers were not observed. Affinities in the scheme were determined from the CG-MALS data from Tables 2 and 3.

Although our results find little support for 2SKp/2CaM, prior reports (Schumacher et al., 2001; Zhang et al., 2012a,b, 2013) mandate that we explore the possibility thoroughly. Our interpretations of CG-MALS data rely on fitting data that have multiple parameters, but the parameters may be correlated, thereby confounding the determination from the fits (unpublished data). We addressed this issue in several ways to increase our confidence in our conclusions.

(1) The molar masses of SKp and CaM can be measured independently during the CG-MALS experiment, and the measurements for molar mass are almost identical to what is predicted for monomers. The fact of whether or not these parameters are fixed or allowed to float during fitting of the hetero-association data does not affect the measured stoichiometries and apparent K_d (Tables 2 and 3). We note that the Calypso software from Wyatt Technologies does not report an uncertainty for the $\log(K_A)$ values from a reversible association fit. We therefore presented ranges that were determined by fixing or floating certain parameters (Tables 2 and 3).

(2) In most modern methods the incompetent fraction is immeasurable and it is usually ignored, but we argue that protein chemists need to consider the amount of incompetent fraction for concentration-sensitive binding studies, especially because MALS appears capable of quantifying it. There is a precedent for including an incompetent fraction during fitting (Attri and Minton, 2005; Hanlon et al., 2010). The inclusion of this term did not affect the measured stoichiometry. It also changed the measured K_d by less than twofold for parameters within instrumental capability (Tables 2 and 3).

(3) There is no rationale for including additional stoichiometries in our models. We attempted to fit other stoichiometries, but the modeled light scattering signal approaches zero for each extra included stoichiometry. However, this obviously doesn't rule out the potential formation of other higher-order associations at high concentrations (outside the range that we studied). A very small proportion of a 2/2 complex at zero Ca^{2+} cannot be definitively ruled out, but there is not enough scattering to be conclusive. Concentrations >15 µM would be required to confirm or rule out this complex, which was outside the scope of our measurement limitations or secondary in importance to the loss of the 1SKp/2CaM complex and a decrease in binding affinity for the second SKp binding site. We also tried to force a 2SKp/2CaM interaction in the presence of calcium during fitting. Unlike the calcium-free case, this term was always thrown out of the "with calcium" fit, no matter what the initial guess was set to be. Using simulation, we can get the same M-shape only if we leave the fitting parameters as they are for the 1SKp/1CaM, 2SKp/1CaM, and 1SKp/2CaM terms and add a 2SKp/2CaM with $\log(K_A) \leq 24$. If we take this $\log(K_A)$ to represent the dimerization of two 1/1 complexes, that leaves a dimerization $K_d \geq 250$ µM. Because we were >100-fold below this concentration, this basically means that under the conditions tested, no 2/2 complex formed, and we would have to increase the concentration by at least 10-fold to see the effect if it exists. To extend this argument, our AUC data went up to at least 250 µM with still no evidence of a 2/2 complex (see point No. 5).

(4) Qualitative features of the data and the fits are consistent with our conclusions. We know the expected masses of all the complexes that form between SKp and CaM, which would most likely form given a molar ratio of SKp:CaM, and how close the calculated mass of a complex comes to reaching the expected mass. In saturating Ca^{2+}, the peak is higher when SKp is in excess than when CaM is in excess, and there is a dip between the two peaks. Physically, this is consistent with the light scattering data only if the K_d for the 2SKp/1CaM is stronger than it is for 1SKp/2CaM and if 1SKp/1CaM forms as the dominant species (>95% of active or "competent" protein) at 1:1 molar ratios with a very strong affinity.

(5) The stoichiometries determined from CG-MALS are fully supported by the AUC data. Because CG-MALS measurements are not affected by molecular shape, we can rule out virtually all exotic arguments that would explain the observations that the complex that forms at 1:1 molar ratios sediments with a smaller coefficient than when molar ratios are unequal; i.e., the complex at 1SKp:1CaM molar ratio sediments with a smaller coefficient because it is in fact smaller than the complexes that form at 1SKp:2CaM or 2SKp:1CaM. Any single approach for measuring the molar mass has experimental limitations and could lead to misinterpretations. Therefore we chose a multifaceted approach to gain confidence in our conclusions. Our results from different techniques are consistent enough to generalize our conclusions.

Why is 2SKp/2CaM not resolved in our data? One explanation would be that the crystal packing environment favors intermolecular contacts that are not favored in a more physiological solution. Alternatively, perhaps the histidine tag altered the formation of the complex in earlier studies (Schumacher et al., 2001). Tags in other proteins have led to some controversy. ERK2 is an extracellular regulated kinase that was believed to be capable of forming dimers, yet it was shown in solution that a histidine tag present in many early studies increases the presence of dimeric complexes of ERK2 (Kaoud et al., 2011). Our approach is to avoid using tags in binding studies whenever possible.

It is important to note that both crystal and solution studies may allow geometries of SKp/CaM that are not encountered when the full SK protein is embedded in

lipid. We conclude from solution studies that the 1 to 1 stoichiometry for CaM to each SK binding site is more consistent with the traditional view of fourfold rotational symmetry of the homotetrameric channel and not the dimeric, twofold symmetry implied with the model derived from a crystal. Thus the basis for using a dimer of dimers model to describe SK gating may not be as relevant as a homotetramer model with fourfold symmetry (Fig. 1 B), which has been predominantly observed in other homotetrameric potassium channels (MacKinnon, 2003).

An unexpected finding is that CaM may have chaperone-like properties with SKp. Although CaM causes SKp to aggregate if the final concentration of CaM is lower than SKp, when the concentration of CaM is greater than that of SKp, aggregation is prevented. When Ca^{2+} is present, no aggregation occurs. CaM has been shown to prevent aggregation and degradation of some small proteins in a Ca^{2+}-dependent manner (Shao and Hegde, 2011).

CaM binding to ion channels senses both local and global changes to Ca^{2+} (Tadross et al., 2008). CaM has been implicated in multiple functions on the same protein as exemplified in VDCCs (Zühlke et al., 1999). Several structures of CaM bound to an IQ motif have been presented among various VDCC that led to various functional interpretations (Fallon et al., 2005; Van Petegem et al., 2005; Mori et al., 2008; Kim et al., 2010). The structures show which residues of the peptides contact CaM in the presence of Ca^{2+} in a crystal environment. However, we know that CaM must have other conformations or move to other sites in order for the channel to sample different functional states (Tadross et al., 2008). A static structure may miss dynamic motions or long-range allosteric effects on binding. Biochemical studies have also shown that residues from VDCC that do not contact CaM in the crystal can still affect Ca^{2+} binding to CaM (Halling et al., 2009). It is not unreasonable to infer that the level of complexity for functional CaM interactions with SK is equally as complex as CaM interactions with VDCC, especially because there are potentially more CaMs involved with SK.

Our data show complexity in the interaction between SKp and CaM. If what we observe with CaM binding to SKp is representative of CaM binding to the full channel, this would suggest that an SK channel may present itself with a range of SK-to-CaM stoichiometry from perhaps 2 to 8 CaM molecules per channel tetramer. Our results can be used to facilitate the interpretation of more complicated findings from future investigations of full-length SK.

We thank Claire Riggs for her excellent technical contributions with light scattering, and Margaux Miller for protein expression and purification. We thank Tom Middendorf, Keegan Hines, Jenni Bernier, and Xixi Chen for comments and helpful suggestions. Thanks to The University of Texas at Austin Institute for Cellular and Molecular Biology facilities for mass spectrometry and for use of the analytical ultracentrifuge. Wyatt provided access to the Calypso/Heleos CG-MALS system. We thank Dr. Borries Demeler and his team for providing workshops on the analytical ultracentrifuge.

AUC data were processed using the UltraScan LIMS cluster at the Bioinformatics Core Facility at The University of Texas Health Science Center at San Antonio and TeraGrid resources, supported by National Science Foundation TeraGrid Grant No. MCB070038 (to Borries Demeler). This research was supported by the National Institutes of Health under Ruth L. Kirschstein National Research Service Award F32GM93626-02 from the National Institute of General Medical Sciences and National Institutes of Health grant NS077821.

The authors have no conflicting financial interests.

Christopher Miller served as editor.

Submitted: 11 April 2013
Accepted: 18 December 2013

REFERENCES

Aon, J.C., R.J. Caimi, A.H. Taylor, Q. Lu, F. Oluboyede, J. Dally, M.D. Kessler, J.J. Kerrigan, T.S. Lewis, L.A. Wysocki, and P.S. Patel. 2008. Suppressing posttranslational gluconoylation of heterologous proteins by metabolic engineering of *Escherichia coli*. *Appl. Environ. Microbiol.* 74:950–958. http://dx.doi.org/10.1128/AEM.01790-07

Attri, A.K., and A.P. Minton. 2005. Composition gradient static light scattering: a new technique for rapid detection and quantitative characterization of reversible macromolecular heteroassociations in solution. *Anal. Biochem.* 346:132–138. http://dx.doi.org/10.1016/j.ab.2005.08.013

Banks, B.E.C., C. Brown, G.M. Burgess, G. Burnstock, M. Claret, T.M. Cocks, and D.H. Jenkinson. 1979. Apamin blocks certain neurotransmitter-induced increases in potassium permeability. *Nature.* 282:415–417. http://dx.doi.org/10.1038/282415a0

Barer, R., and S. Joseph. 1954. Refractometry of living cells: Part I. Basic principles. *Quarterly Journal of Microscopical Science.* 95:399–423.

Bernhardt, J., and H. Pauly. 1975. Partial specific volumes in highly concentrated protein solutions. I. Water-bovine serum albumin and water-bovine hemoglobin. *J. Phys. Chem.* 79:584–590. http://dx.doi.org/10.1021/j100573a010

Brookes, E., W. Cao, and B. Demeler. 2010. A two-dimensional spectrum analysis for sedimentation velocity experiments of mixtures with heterogeneity in molecular weight and shape. *Eur. Biophys. J.* 39:405–414. http://dx.doi.org/10.1007/s00249-009-0413-5

Callaway, K.A., M.A. Rainey, A.F. Riggs, O. Abramczyk, and K.N. Dalby. 2006. Properties and regulation of a transiently assembled ERK2. Ets-1 signaling complex. *Biochemistry.* 45:13719–13733. http://dx.doi.org/10.1021/bi0610451

Cantor, R.C., and P.R. Schimmel. 1980. Biophysical Chemistry. Part 2: Techniques for the Study of Biological Structure and Function. W. H. Freeman and Company, San Francisco.

Cao, W., and B. Demeler. 2005. Modeling analytical ultracentrifugation experiments with an adaptive space-time finite element solution of the Lamm equation. *Biophys. J.* 89:1589–1602. http://dx.doi.org/10.1529/biophysj.105.061135

Debye, P. 1944. Light scattering in solutions. *J. Appl. Phys.* 15:338. http://dx.doi.org/10.1063/1.1707436

Demeler, B., and K.E. van Holde. 2004. Sedimentation velocity analysis of highly heterogeneous systems. *Anal. Biochem.* 335:279–288. http://dx.doi.org/10.1016/j.ab.2004.08.039

Demeler, B., E. Brookes, R. Wang, V. Schirf, and C.A. Kim. 2010. Characterization of reversible associations by sedimentation velocity with UltraScan. *Macromol. Biosci.* 10:775–782. http://dx.doi.org/10.1002/mabi.200900481

Edelhoch, H. 1967. Spectroscopic determination of tryptophan and tyrosine in proteins. *Biochemistry.* 6:1948–1954. http://dx.doi.org/10.1021/bi00859a010

Fallon, J.L., D.B. Halling, S.L. Hamilton, and F.A. Quiocho. 2005. Structure of calmodulin bound to the hydrophobic IQ domain of the cardiac $Ca_v1.2$ calcium channel. *Structure.* 13:1881–1886. http://dx.doi.org/10.1016/j.str.2005.09.021

Geoghegan, K.F., H.B. Dixon, P.J. Rosner, L.R. Hoth, A.J. Lanzetti, K.A. Borzilleri, E.S. Marr, L.H. Pezzullo, L.B. Martin, P.K. LeMotte, et al. 1999. Spontaneous alpha-N-6-phosphogluconoylation of a "His tag" in *Escherichia coli*: the cause of extra mass of 258 or 178 Da in fusion proteins. *Anal. Biochem.* 267:169–184. http://dx.doi.org/10.1006/abio.1998.2990

Halling, D.B., P. Aracena-Parks, and S.L. Hamilton. 2006. Regulation of voltage-gated Ca^{2+} channels by calmodulin. *Sci. STKE.* 2006:er1.

Halling, D.B., D.K. Georgiou, D.J. Black, G. Yang, J.L. Fallon, F.A. Quiocho, S.E. Pedersen, and S.L. Hamilton. 2009. Determinants in Ca_V1 channels that regulate the Ca^{2+} sensitivity of bound calmodulin. *J. Biol. Chem.* 284:20041–20051. http://dx.doi.org/10.1074/jbc.M109.013326

Hanlon, A.D., M.I. Larkin, and R.M. Reddick. 2010. Free-solution, label-free protein-protein interactions characterized by dynamic light scattering. *Biophys. J.* 98:297–304. http://dx.doi.org/10.1016/j.bpj.2009.09.061

Jurado, L.A., P.S. Chockalingam, and H.W. Jarrett. 1999. Apocalmodulin. *Physiol. Rev.* 79:661–682.

Kaoud, T.S., A.K. Devkota, R. Harris, M.S. Rana, O. Abramczyk, M. Warthaka, S. Lee, M.E. Girvin, A.F. Riggs, and K.N. Dalby. 2011. Activated ERK2 is a monomer in vitro with or without divalent cations and when complexed to the cytoplasmic scaffold PEA-15. *Biochemistry.* 50:4568–4578. http://dx.doi.org/10.1021/bi200202y

Keen, J.E., R. Khawaled, D.L. Farrens, T. Neelands, A. Rivard, C.T. Bond, A. Janowsky, B. Fakler, J.P. Adelman, and J. Maylie. 1999. Domains responsible for constitutive and Ca(2+)-dependent interactions between calmodulin and small conductance Ca(2+)-activated potassium channels. *J. Neurosci.* 19:8830–8838.

Kim, E.Y., C.H. Rumpf, F. Van Petegem, R.J. Arant, F. Findeisen, E.S. Cooley, E.Y. Isacoff, and D.L. Minor Jr. 2010. Multiple C-terminal tail Ca^{2+}/CaMs regulate $Ca_V1.2$ function but do not mediate channel dimerization. *EMBO J.* 29:3924–3938. http://dx.doi.org/10.1038/emboj.2010.260

Lamm, O. 1929. Die differentialgleichung der ultrazentrifugierung. *Arkiv för Matematik, Astronomi Och Fysik.* 21B:1–4.

Laue, T.M., and W.F. Stafford III. 1999. Modern applications of analytical ultracentrifugation. *Annu. Rev. Biophys. Biomol. Struct.* 28:75–100. http://dx.doi.org/10.1146/annurev.biophys.28.1.75

Lewis, G.N., and M. Randall. 1961. Solutions. *In* Thermodynamics, Second edition. McGraw-Hill Book Company, Inc., New York. 199–223 pp.

Li, W., D.B. Halling, A.W. Hall, and R.W. Aldrich. 2009. EF hands at the N-lobe of calmodulin are required for both SK channel gating and stable SK-calmodulin interaction. *J. Gen. Physiol.* 134:281–293. http://dx.doi.org/10.1085/jgp.200910295

MacKinnon, R. 2003. Potassium channels. *FEBS Lett.* 555:62–65. http://dx.doi.org/10.1016/S0014-5793(03)01104-9

Marshak, D.R. 1996. Strategies for Protein Purification and Characterization: a Laboratory Course Manual. Cold Spring Harbor Laboratory Press, Cold Spring Harbor, NY. 396 pp.

Mori, M.X., C.W. Vander Kooi, D.J. Leahy, and D.T. Yue. 2008. Crystal structure of the Ca_V2 IQ domain in complex with Ca^{2+}/calmodulin: high-resolution mechanistic implications for channel regulation by Ca^{2+}. *Structure.* 16:607–620. http://dx.doi.org/10.1016/j.str.2008.01.011

Pitman, E.J.G. 1937. Significance tests which may be applied to samples from any populations. *Supplement to the Journal of the Royal Statistical Society.* 4:119–130. http://dx.doi.org/10.2307/2984124

Schoenmakers, T.J., G.J. Visser, G. Flik, and A.P. Theuvenet. 1992. CHELATOR: an improved method for computing metal ion concentrations in physiological solutions. *Biotechniques.* 12:870–874: 876–879.

Schuck, P. 2000. Size-distribution analysis of macromolecules by sedimentation velocity ultracentrifugation and lamm equation modeling. *Biophys. J.* 78:1606–1619. http://dx.doi.org/10.1016/S0006-3495(00)76713-0

Schumacher, M.A., A.F. Rivard, H.P. Bächinger, and J.P. Adelman. 2001. Structure of the gating domain of a Ca^{2+}-activated K^+ channel complexed with Ca^{2+}/calmodulin. *Nature.* 410:1120–1124. http://dx.doi.org/10.1038/35074145

Shao, S., and R.S. Hegde. 2011. A calmodulin-dependent translocation pathway for small secretory proteins. *Cell.* 147:1576–1588. http://dx.doi.org/10.1016/j.cell.2011.11.048

Slotboom, D.J., R.H. Duurkens, K. Olieman, and G.B. Erkens. 2008. Static light scattering to characterize membrane proteins in detergent solution. *Methods.* 46:73–82. http://dx.doi.org/10.1016/j.ymeth.2008.06.012

Stafford, W.F. III. 1992. Boundary analysis in sedimentation transport experiments: a procedure for obtaining sedimentation coefficient distributions using the time derivative of the concentration profile. *Anal. Biochem.* 203:295–301. http://dx.doi.org/10.1016/0003-2697(92)90316-Y

Tadross, M.R., I.E. Dick, and D.T. Yue. 2008. Mechanism of local and global Ca^{2+} sensing by calmodulin in complex with a Ca^{2+} channel. *Cell.* 133:1228–1240. http://dx.doi.org/10.1016/j.cell.2008.05.025

Van Holde, K.E., and W.O. Weischet. 1978. Boundary analysis of sedimentation-velocity experiments with monodisperse and paucidisperse solutes. *Biopolymers.* 17:1387–1403. http://dx.doi.org/10.1002/bip.1978.360170602

Van Petegem, F., F.C. Chatelain, and D.L. Minor Jr. 2005. Insights into voltage-gated calcium channel regulation from the structure of the $Ca_V1.2$ IQ domain-Ca^{2+}/calmodulin complex. *Nat. Struct. Mol. Biol.* 12:1108–1115. http://dx.doi.org/10.1038/nsmb1027

Wang, Y., I. Teraoka, F.Y. Hansen, G.H. Peters, and O. Hassager. 2010. A theoretical study of the separation principle in size exclusion chromatography. *Macromolecules.* 43:1651–1659. http://dx.doi.org/10.1021/ma902377g

Wissmann, R., W. Bildl, H. Neumann, A.F. Rivard, N. Klöcker, D. Weitz, U. Schulte, J.P. Adelman, D. Bentrop, and B. Fakler. 2002. A helical region in the C terminus of small-conductance Ca^{2+}-activated K^+ channels controls assembly with apo-calmodulin. *J. Biol. Chem.* 277:4558–4564. http://dx.doi.org/10.1074/jbc.M109240200

Wyatt, P.J. 1993. Light scattering and the absolute characterization of macromolecules. *Anal. Chim. Acta.* 272:1–40. http://dx.doi.org/10.1016/0003-2670(93)80373-S

Xia, X.-M., B. Fakler, A. Rivard, G. Wayman, T. Johnson-Pais, J.E. Keen, T. Ishii, B. Hirschberg, C.T. Bond, S. Lutsenko, et al. 1998. Mechanism of calcium gating in small-conductance calcium-activated potassium channels. *Nature.* 395:503–507. http://dx.doi.org/10.1038/26758

Yamniuk, A.P., and H.J. Vogel. 2004. Calmodulin's flexibility allows for promiscuity in its interactions with target proteins and peptides. *Mol. Biotechnol.* 27:33–57. http://dx.doi.org/10.1385/MB:27:1:33

Zhang, M., C. Abrams, L. Wang, A. Gizzi, L. He, R. Lin, Y. Chen, P.J. Loll, J.M. Pascal, and J.F. Zhang. 2012a. Structural basis for calmodulin as a dynamic calcium sensor. *Structure.* 20:911–923. http://dx.doi.org/10.1016/j.str.2012.03.019

Zhang, M., J.M. Pascal, M. Schumann, R.S. Armen, and J.F. Zhang. 2012b. Identification of the functional binding pocket for compounds targeting small-conductance Ca^{2+}-activated potassium channels. *Nat Commun.* 3:1021. http://dx.doi.org/10.1038/ncomms2017

Zhang, M., J.M. Pascal, and J.-F. Zhang. 2013. Unstructured to structured transition of an intrinsically disordered protein peptide in coupling Ca^{2+}-sensing and SK channel activation. *Proc. Natl. Acad. Sci. USA.* 110:4828–4833. http://dx.doi.org/10.1073/pnas.1220253110

Zhu, H., D.W. Ownby, C.K. Riggs, N.J. Nolasco, J.K. Stoops, and A.F. Riggs. 1996. Assembly of the gigantic hemoglobin of the earthworm *Lumbricus terrestris.* Roles of subunit equilibria, nonglobin linker chains, and valence of the heme iron. *J. Biol. Chem.* 271:30007–30021. http://dx.doi.org/10.1074/jbc.271.47.30007

Zimm, B.H. 1948. The dependence of the scattering of light on angle and concentration in linear polymer solutions. *J. Phys. Colloid Chem.* 52:260–267. http://dx.doi.org/10.1021/j150457a022

Zühlke, R.D., G.S. Pitt, K. Deisseroth, R.W. Tsien, and H. Reuter. 1999. Calmodulin supports both inactivation and facilitation of L-type calcium channels. *Nature.* 399:159–162. http://dx.doi.org/10.1038/20200